

"Dissemination of Education for Knowledge, Science and Culture"  
- Shikshanmaharshi Dr. Bapuji Salunkhe  
Shri Swami Vivekanand Shikshan Sanstha's

## **Vivekanand College, Kolhapur**

### **Department of Physics**

#### **M.Sc. II Student Research Project (2024 – 25)**

<b>Sr. No.</b>	<b>Name of the Student</b>	<b>Research Project Title</b>
1.	Bhingardeve Dhiraj Prakash	Characterization and synthesis of nickel magnesium ferrite by sol-gel autocombustion method
2.	Devkule Nishiganda Nishikant	Self-focusing/defocusing collisional and collisionless plasma
3.	Dongare Suyash Sanjay	Preparation and characterization of CdS thin film by CBD method
4.	Gavade Gouri Balasaheb	Synthesis and characterization of copper oxide thin film by SILAR method
5.	Jamadar Mahek Shakilahmed	Fabrication of silica-PTFE based transparent superhydrophobic coating on glass substrate for self-cleaning and photovoltaic applications
6.	Kamble Anjali Bhagwan	Synthesis and characterization of $Ba_{1-x}La_xFe_2O_4$ prepared by sol-gel autocombustion method
7.	Kavathekar Akash Bhimrao	Superhydrophobic polycarbonate material for self-cleaning applications
8.	Yadhav Vedaja Ajay	Photothermal superhydrophobic polyaniline-polymer nanocomposite coating on cotton fabric for self-cleaning and self-sterilization applications



*sslatte*  
**HEAD**  
**DEPARTMENT OF PHYSICS**  
**VIVEKANAND COLLEGE, KOLHAPUR**  
**(EMPOWERED AUTONOMY)**



"Dissemination of Education for Knowledge, Science and Culture"

Shikshanmaharshi Dr. BapujiSalunkhe

**Characterization and synthesis of nickel magnesium ferrite  
By Sol-gel autocombustion Method**

A Research Project Submitted To

**VIVEKANAND COLLEGE (AUTONOMOUS),  
KOLHAPUR**

FOR THE DEGREE OF MASTER OF SCIENCE

IN

PHYSICS

**UNDER THE FACULTY OF SCIENCE**

BY

**Mr. Dhiraj Prakash Bhingardev  
(Msc - II)**

UNDER THE GUIDENCE OF

**Mr. A . R . Gaikwad  
(Msc , SET, GATE)**

**DEPARTMENT OF PHYSICS**

VIVEKANAND COLLEGE KOLHAPUR

(EMPOWERED AUTONOMOUS)

2024 - 2025

## CERTIFICATE

This is to certify that the project entitled " **Characterization and synthesis of nickel magnesium ferrite By Sol-gel autocombustion Method** " being submitted herewith for the award of the degree of Master of Science in Physics of Vivekanand College, Kolhapur [Empowered Autonomous] is the result of the original research work done by Mr. Dhiraj Prakash Bhingardev under my/our knowledge and belief the work embodied in this project has not formed earlier the basis for the award of any degree of similar title of this or any other University or Examining body.

Place: Kolhapur

Date:

29/04/2025



(Mr. A. R. Gaikwad)  
Msc, SET

(Project Guide)

DEPARTMENT OF PHYSICS

Vivekanand College, Kolhapur  
[Empowered Autonomous]

  
Examiner

Head

DEPARTMENT OF PHYSICS

Vivekanand College, Kolhapur  
[Empowered Autonomous]

### DECLARATION BY STUDENT

I hereby declare that the project entitled "**Characterization and synthesis of nickel magnesium ferrite By Sol-gel autocombustion Method**" completed and written by me and has neither formed earlier the basis for the award of any degree of similar title of this nor any other University nor Examining body. Further, I declare that I have not violated any of the provisions under Copyright Privacy/Cyber/IPR Act as and when amended from time to time.

Place: Kolhapur

Date:

  
Mr. DhiraJ Prakash Bhingardev

Project      Student

## ACKNOWLEDGEMENT

I have great pleasure to express my deep sense of indebtedness and heart of full gratitude to my project guide Mr. A. R. Gaikwad, Department of Physics, of Vivekanand College, Kolhapur [Empowered Autonomous] for his valuable guidance given to me during the course of project work.

I am very grateful to Dr. S. S. Lathe, Head of Department of Physics, Vivekanand College, Kolhapur [Empowered Autonomous] for making available chemicals, materials, laboratory facilities and his inspiration towards a common goal of achieving scientific knowledge and pursuit it.

I wish to express my appreciation to Mr. Rushiraj Supale for their discussion and cooperation in each and every moment of project work.



## Index

Sr. No.	Chapter Name	Page No.
1	Introduction and theoretical background	2
2	Synthesis of $\text{Ni}_{1-x}\text{Mg}_x\text{Fe}_2\text{O}_4$	17
3	Literature survey	23
4	characterization techniques	25
5	Summary and conclusion	28

## **Chapter 1: Introduction and theoretical background**

### **1.1 History of ferrite**

### **1.2 Introduction to ferrites**

### **1.3 Types of Ferrites**

#### **1.3.1 Spinel ferrite**

#### **1.3.2 Hexagonal ferrite**

#### **1.3.3 Ortho Ferrite**

#### **1.3.4 Garnet Ferrite**

### **1.4 Applications of Ferrite**

#### **1.4.1 High Frequency**

#### **1.4.2 Power**

#### **1.4.3 Electromagnetic Interference (EMI) Suppression**

#### **1.4.4 Biosciences**

## 1.1 History of ferrite

The history of ferrite, also known as magnetic oxide, dates back to centuries before the birth of Christ, when stones that could attract iron were first discovered. For more than 2,500 years, humans have harnessed magnetism for a wide range of purposes, including navigation, energy, manufacturing, and advanced technologies. Magnetism has become such a familiar concept that, since the time of Thales of Miletus, the terms "magnetic" and "attracted" have often been used interchangeably. Scientific explanations of magnetism sometimes venture into the realm of the abstract, as seen in the concept of "spin," which emerged from Dirac's relativistic model of an electron in an external magnetic field. This concept has become fundamental to our modern understanding of magnetism, where the spin of electrons creates a magnetic moment, and the motion of electric charges contributes to an orbital magnetic moment.

The first known mention of magnetism in Chinese records is attributed to Guan Zhong around 645 BC, with later texts also referencing lodestone. In China, lodestone was called "cishi," meaning "loving stone," due to its magnetic attraction to iron. During the Qin dynasty (221–206 BC), directional tools were created by balancing lodestone pieces. One such device was a spoon-shaped piece of lodestone placed on a bronze plate, with its handle pointing south. These instruments were likely used for Feng Shui or geomancy, ancient practices aimed at harmonizing with natural forces, rather than for navigation. A later reference to the compass appears in Shen Kuo's *Meng Xi Bi Tan* (1086 AD), where he described a compass needle pointing south and also notes a slight easterly deviation, indicating a change in the compass's direction.

Medieval European literature also tells stories about magnetic mountains or islands, believed to have the power to pull copper or bronze nails out of boats. In 1780, F. A. Mesmer developed a healing technique based on the idea that living beings are magnetized and can be healed through magnetic fields. In 1819, Hans Christian Oersted discovered that an electric current in a wire influences the needle of a magnetic compass. With additional contributions from Faraday, Maxwell, Hertz, and others, the field of electromagnetism was established. ng south and noted a slight eastward deviation, an early observation of magnetic declination.

In 1930, Yogoro and Takeshi from the Institute of Technology in Tokyo synthesized the first ferrite compound. Naturally occurring magnetite is a weak form of 'hard' ferrite, which



has the necessary magnetism to remain permanent. Over time, human-made 'hard' ferrites with enhanced properties were developed, while creating a corresponding 'soft' magnetic material in the laboratory was successfully achieved.

## 1.2 Introduction to ferrites

Many inorganic oxides form a face-centered cubic (FCC) lattice of  $O^{2-}$  ions, with interstitial cations holding the structure together. Within this lattice, there are two types of interstitial sites: tetrahedral sites, where a cation is surrounded by four nearest neighbors, and octahedral sites, where a cation is surrounded by six nearest neighbors. If all the tetrahedral sites are empty and the octahedral sites are filled, the structure adopts a rock salt arrangement. Conversely, if only the tetrahedral sites are filled, the structure follows a zinc-blende pattern. In spinel ferrites, cations are distributed across both tetrahedral and octahedral sites, with twice as many octahedral sites being filled as tetrahedral ones. This creates a structure that can be seen as a combination of the zinc-blende and rock-salt configurations, which contributes to the unique properties of spinel ferrites used in various applications.

Ferrites possess semiconducting properties, which are crucial in various technological applications due to their magnetic and electrical characteristics. They are used in sensors, transformer cores, antenna rods, memory chips, high-density magnetic recording media, transducers, permanent magnets, activators, memory sensors, microwave systems, communication technologies, and computer systems. The nanocrystalline form of ferrite has found applications in areas such as magnetically guided drug delivery, catalysts, magnetic resonance imaging (MRI), humidity and gas sensors, and magnetic fluids. Another key feature of ferrites, which is largely insignificant in metals, is their porosity. Additionally, ferrites exhibit dielectric properties, further enhancing their utility in various technological fields.

Ferrites have dielectric properties, allowing electromagnetic waves to pass through them while not readily conducting electricity. This characteristic gives ferrites an advantage over metals like iron, nickel, and other transition metals, which also possess magnetic properties but conduct electricity. The combination of various properties of ferrites explains why they have been studied and used for many years. With the growing demand for ferrite

technology, the properties of ferrites have been continuously modified and improved. It is believed that ferrite technologies and applications have a promising future. Ferrites are electrically non-conductive, making them insulators, and they are ferrimagnetic, meaning they can easily be magnetized or attracted to a magnet. Depending on their resistance to demagnetization, ferrites can be classified into two categories. Ferrite compounds are low-cost, primarily made from rusted iron (iron oxide), and have excellent corrosion resistance. They are highly stable, difficult to demagnetize, and can be manufactured with both high and low coercive forces.

Transition metal ferrite nanoparticles have garnered significant attention due to their unique properties, which make them suitable for applications in areas like magnetic storage, biomedicine, ferrofluids, catalysis, and magnetic refrigeration systems. Recent advancements in physics have led to progress in innovative technologies and scientific developments. Hard ferrites, which have high coercivity, are difficult to demagnetize. These are commonly used to produce permanent magnets for applications such as refrigerator magnets, loudspeakers, and small electric motors. On the other hand, soft ferrites have low coercivity, allowing them to easily change their magnetization, which makes them effective conductors of magnetic fields. These are widely used in the electronics industry to create efficient magnetic cores, known as ferrite cores, for high-frequency inductors, transformers, antennas, and various microwave components.

Ferrites are generally classified into three types: spinel, garnet, and magneto-plumbite, each with its distinct characteristics and significance for technological applications. Magneto-plumbite ferrites, typically represented as  $MFe_2O_4$  (where M can be Ba, Sr, Ca, etc.), are particularly important in permanent magnet applications. Garnet ferrites, with the formula  $R_3Fe_5O_{12}$  (where R is a rare earth ion like Yttrium, Dy, or La), find applications in microwave systems. Spinel ferrites are commonly represented by the chemical formula  $MFe_2O_4$ , where M is a divalent cation such as Co, Ni, Zn, or Cd. The crystal structure of spinel ferrites is based on a cubic close-packed arrangement of oxygen ions, and it features two types of interstitial sites: tetrahedral (A) and octahedral (B). These sites can accommodate cations with different valences and ionic radii, contributing to the unique properties of spinel ferrites.



### 1.3 Types of Ferrites

Ferrites can be classified into three different types

1. Spinel ferrite (cubic ferrite)
2. Hexagonal ferrite
3. Ortho ferrite
4. Garnet ferrite

The taken compound is of spinel ferrite type hence we are discussing spinel ferrite in detail and introduction to others two.

#### 1.3.1 Spinel ferrite

In many inorganic oxides, the oxygen ions ( $O^{2-}$ ) form a face-centered cubic (FCC) lattice, and the structure is stabilized by interstitial cations. Within this FCC lattice, there are two primary types of interstitial sites: tetrahedral sites, where a cation has four nearest neighbors, and octahedral sites, where a cation has six nearest neighbors. If all tetrahedral sites are left vacant and all octahedral sites are filled, the structure adopts a rock salt arrangement. On the other hand, if only the tetrahedral sites are filled, the structure adopts a zinc-blende configuration.

In the case of spinel ferrites, cations occupy both tetrahedral and octahedral interstitial sites. Notably, twice as many octahedral sites are occupied as tetrahedral sites, giving the spinel structure a unique characteristic. The spinel lattice can be viewed as an ordered blend of both the zinc-blende and rock-salt structures. This arrangement contributes to the distinctive properties of spinel ferrites, making them useful in various applications, particularly in magnetism and electronics.

The cubic unit cell of spinel compounds contains eight smaller cubes, also referred to as octants or formula units, which correspond to the formula  $A_8B_{16}O_{32}$ . Bragg and Nishikawa were the first to determine the spinel structure. In this structure, the oxygen anions form a face-centered cubic (FCC) close packing, with the cations partially occupying the tetrahedral and octahedral interstices. The tetrahedral interstices are situated at the center of a tetrahedron formed by four oxygen atoms.

In a single plane, three oxygen ions are in contact with each other, while the fourth oxygen atom is positioned symmetrically on top, at the center of the plane containing the three anions.

The chemical composition of a given spinel ferrite can generally be written as  $M_xFe_{12}O_4M_xFe_{12}O_4$ , where M represents a divalent metal ion such as  $Co^{2+}$ ,  $Zn^{2+}$ ,  $Fe^{2+}$ ,  $Mg^{2+}$ ,  $Ni^{2+}$ ,  $Cd^{2+}$ ,  $Cu^{2+}$ , or a combination of these ions. The unit cell of spinel ferrite is FCC, with eight formula units per unit cell. The formula can be expressed as  $M_xFe_8O_4M_xFe_8O_4$ , with the oxygen anions forming the FCC lattice. Within this lattice, two types of interstitial positions exist, and these are occupied by the metallic cations.

The unit cell of spinel ferrites contains 96 interstitial sites, which are distributed as 64 tetrahedral (A) sites and 32 octahedral (B) sites. Ferrites can be considered as solid solutions, with examples of inverse ferrites such as  $NiFe_2O_4$  and  $CuFe_2O_4$ , and normal ferrites like  $ZnFe_2O_4$ . Due to favorable charge distribution,  $Ni^{2+}$  and  $Cu^{2+}$  ions tend to prefer the octahedral B-site, while  $Zn^{2+}$  ions strongly favor the tetrahedral A-site because of their electronic configuration. Non-crystalline (NCZ) spinel ferrites are easy to prepare and are commercially attractive due to their versatility in various applications. Due to their high electrical resistivity and strong magnetic properties at higher frequencies, these ferrites are used in surface mount devices (SMDs) and multilayer chip inductors (MLCIs). Spinel ferrites are classified into three types based on how the cations are distributed across the tetrahedral (A) and octahedral (B) sites.

- a) Normal spinel ferrite
- b) Inverse spinel ferrite
- c) Intermediate spinel ferrites.

#### **a) Normal Spinel**

If only one type of cation occupies the octahedral [B] site, the spinel is classified as normal. In these ferrites, the divalent cations occupy the tetrahedral (A) sites, while the trivalent cations are positioned on the octahedral [B] sites. Square brackets are used to denote the ionic

distribution in the octahedral [B] sites. Normal spinel ferrites are typically represented by the formula  $(M^{2+})_A[Me^{3+}]_B O_4$ , where  $M^{2+}$  represents the divalent ions and  $Me^{3+}$  represents the trivalent ions. A typical example of a normal spinel ferrite is bulk zinc ferrite.

#### b) Inverse spinel

In this structure, half of the trivalent ions occupy the tetrahedral (A) sites, while the other half occupy the octahedral (B) sites, with the remaining cations being randomly distributed among the octahedral [B] sites. These ferrites are represented by the formula  $(Me^{3+})_A(M^{2+}-Me^{3+})_B O_4$ . A typical example of an inverse spinel ferrite is iron oxide  $Fe_3O_4$ , where the divalent iron ions ( $Fe^{2+}$ ) occupy the octahedral [B] sites, and the trivalent iron ions ( $Fe^{3+}$ ) occupy both tetrahedral (A) and octahedral (B) sites.

#### c) Random spinel

Spinel ferrites with an ionic distribution that is intermediate between normal and inverse spinels are known as mixed or random spinels. The inversion parameter, denoted by  $D$ , describes the degree of inversion in the ferrite structure. The value of  $D$  depends on the method of preparation and the nature of the ferrite constituents. For a completely normal spinel ferrite,  $D=0$ , while for a completely inverse spinel ferrite,  $D=1$ . For mixed spinel ferrites,  $D$  ranges between these two extreme values. In the case of a completely mixed ferrite,  $D=0.5$ . If there is an unequal number of each type of cation on the octahedral sites, the spinel is classified as mixed. Typical examples of mixed spinel ferrites include magnesium ferrite  $MgFe_2O_4$  and manganese ferrite  $MnFe_2O_4$ .

Neel proposed that the magnetic moment in ferrites is the sum of the magnetic moments of the individual sub-lattices. In the spinel structure, there are varying exchange interactions between the electrons of ions at the A and B sites. It has been found that the interaction between magnetic ions on the A and B sites (AB-site interaction) is the strongest. The interaction between ions at AA sites is about ten times weaker than the AB-site interaction, while the interaction at BB sites is the weakest. Complete or partial antiferromagnetism, which results from the dominant AB-site interaction, is known as ferrimagnetism. The dominant AB-site interaction, which possesses the greatest exchange energy, leads to an antiparallel arrangement



of cations between the magnetic moments of the two sub-lattices, while maintaining a parallel arrangement of cations within each sub-lattice. This occurs even though there are AA-site or BB-site anti-ferrimagnetic interactions.

### 1.3.2 Hexagonal ferrite

Hexagonal ferrites were first recognized in 1952, and many ferrites with a hexagonal structure have gained significant importance in recent years for various technological applications. These ferrites are further sub-classified into M, W, Y, Z, and U compounds. The M-type compounds have the simplest structure, and barium ferrite, a hard ferrite, belongs to this M-type. These compounds have the general formula  $\text{MeFe}_2\text{O}_9$ , where Me represents a divalent ion with a large ionic radius, such as  $\text{Ba}^{2+}$ ,  $\text{Sr}^{2+}$ , or  $\text{Pb}^{2+}$ . The oxygen ions in these ferrites form a close-packed hexagonal crystal structure.

M-type hexagonal ferrites are typically used as permanent magnets due to their high coercivity and ability to operate at very high frequencies. While the spinel structure with closely packed oxygen ions is similar to the hexagonal ferrite lattice, hexagonal ferrites also include metal ions in some layers that have similar ionic radii to the oxygen ions. This replacement of oxygen ions with larger ions such as barium, strontium, or lead makes hexagonal ferrites larger than garnet ferrites.

### 1.3.3 Ortho Ferrite

Ferrites with the general formula  $\text{RFeO}_3$  are known as orthoferrites, where R is a large trivalent metal ion, such as rare-earth ions or Yttrium (Y). These ferrites crystallize in a distorted perovskite structure, similar to the  $\text{CaTiO}_3$  structure, with an orthorhombic unit cell and exhibit weak ferromagnetism. Although the canting angle of the spins is small, on the order of  $10^{-2}$  radians, it is enough to create a small net ferromagnetic moment perpendicular to the antiferromagnetic axis.

At room temperature, the spin orientation of the Fe ions in  $\text{HoFeO}_3$  and  $\text{ErFeO}_3$  has been experimentally determined to be parallel to the (100) axis. As the temperature decreases, the

spin axis rotates, and at lower Néel temperatures (6.5 K for  $\text{HoFeO}_3$  and 4.3 K for  $\text{ErFeO}_3$ ), the spin moments of the rare-earth ions become ordered.

Orthoferrites are transparent and can modify the polarization of light under the influence of a magnetic field. This makes them potential candidates for use as optical sensors and actuators in optical communications. They were also once used as magnetic materials in bubble memory systems.

### 1.3.4 Garnet Ferrite

Ferrimagnetic garnets are a type of ferrite with the general chemical formula  $\text{R}_3\text{Fe}_5\text{O}_{12}$ , where RRR represents a trivalent ion such as a rare-earth ion or yttrium. In these ferrites, the RRR ions occupy dodecahedral sites (also called e sites), which have twelve plane faces and are surrounded by eight oxygen ions. The iron (Fe) ions are distributed over the tetrahedral and octahedral sites in a ratio of 3:2. The cation distribution in these ferrites can be written as  $\text{M}^{2+}\text{Fe}_3\text{O}_{12}\text{M}^{3+}\text{Fe}_2\text{O}_{12}\text{M}^{3+}\text{Fe}_3\text{O}_{12}$ .

As in the case of spinels, the magnetic alignment in garnets results from super exchange interactions mediated by the intervening oxygen ions. The unit cell of ferrimagnetic garnets is cubic and contains eight molecules of  $\text{M}^{2+}\text{Fe}_3\text{O}_{12}\text{M}^{3+}\text{Fe}_2\text{O}_{12}\text{M}^{3+}\text{Fe}_3\text{O}_{12}$ , which is equivalent to 160 atoms. The metal ions are distributed across three types of sites in the structure.

In 1951, Yoder and Keith discovered that substitutions could be made in the ideal mineral garnet, such as  $\text{MgAl}_2\text{SiO}_2\text{MgAl}_2\text{SiO}_2$ . They created the first silicon-free garnet,  $\text{Y}_3\text{Al}_5\text{O}_{12}$ , by substituting  $\text{Y}^{3+}$  for  $\text{Mg}^{2+}$  and  $\text{Al}^{3+}$  for  $\text{Si}^{4+}$ . The crystal structure of  $\text{Y}_3\text{Al}_5\text{O}_{12}$  is cubic, with an edge length of approximately 12.5 Å, showing a complex arrangement. These ferrimagnetic garnets are important due to their applications in memory structures and other technological fields.

## 1.4 Applications of Ferrite

Ferrites have a wide array of applications, with spinel ferrite ceramics being particularly valuable in microwave devices. These materials are used to control the transmission path, frequency, amplitude, and phase of microwave signals. To optimize the development of these devices and support the efficient manufacturing of ferrites, it is crucial to accurately measure their dielectric and magnetic properties across the relevant frequency and temperature ranges. Structured magnetic materials, such as ferrites, are a fascinating subject of study due to their diverse applications that span a range of industries, from information technology to biotechnology.

Multi-layer capacitors entered the market a recent decades ago, while anos entond in the 1980s. The primary components to produce the inductance is very soft Fe and amma coil. Also, ferrite film should be prepared by a process compatible with the negrated con manufacturing process, to provide a high permeability at that operation fimumcy Spring gives films with high density, but the composition is sometimes not easy to come wit accuracy, and the annealing processes can reach to high temperames. Pulsed laser dep gives high-quality films. Ferrites are excellent soft magnetic materials for high-frequency devices due to their low cost, high resistivity, and low eddy current losses. These properties have made them extensively studied for multilayer chip inductor (MLCI) applications. Ni-Cu-Zn ferrites, in particular, have evolved to support the miniaturization of electronic components. Ferrites are primarily used as inductive components in a variety of electronic circuits, including low-noise amplifiers, filters, voltage-controlled oscillators, and impedance matching networks, among others. Recently, their use in inductors has expanded in line with trends toward miniaturization and integration, particularly in ferrite multilayers for passive functional electronic devices. The multilayer technology has become a crucial advancement in mass production of integrated devices, as it enables a high degree of integration density.

### 1.4.1 High Frequency

Recently, there has been an increased demand for high-frequency applications of magnetic materials in fields such as telecommunications and radar systems, as microwave technology requires higher frequencies and bandwidths of up to 100 GHz. Ferrites are ideal for



these applications because, as non-conducting oxides, they allow the full penetration of electromagnetic fields, unlike metals, which limit the penetration of high-frequency fields due to the skin effect. At such high frequencies, domain walls in ferrites can follow the fields (with domain dispersion occurring around 10 GHz), and microwave power absorption takes place via spin dynamics.

In typical high-frequency devices, spins are first aligned with a DC magnetic field  $H_{DC}$ , and then the microwave field is applied perpendicular to  $H_{DC}$ . Some common high-frequency devices include circulators, isolators, phase shifters, and antennas. Circulators, initially developed for radar systems, are now widely used in mobile phones. They allow the same device to be used for both the transmission and reception of the response signal.

#### 1.4.2 Power

Ferrites play a crucial role in power applications, especially in power supplies for a wide range of devices such as computers, TVs, video systems, and various minor and medium-sized instruments. One of the most important applications is in switched-mode power supplies (SMPS). In this process, the mains power signal is first rectified and then switched as regular pulses (typically rectangular) at a high frequency to supply power to a ferrite transformer. The signal is then rectified again to provide the required amount of power to the device. By increasing the working frequency of the transformer, both power delivery and efficiency can be improved.

A recent approach to enhancing the efficiency of ferrite cores focuses on increasing resistivity, which reduces eddy currents. However, in high-temperature power applications, such as those used in automotive power devices, an additional challenge arises. The working temperature increases due to proximity to the car engine, which affects performance. To address this, ferrite thin films and stencil-printed ceramic-polymer composites have been investigated. This approach combines the excellent magnetic properties of ferrites with the processing advantages of polymer thick films, offering potential for improved performance in demanding power applications.

Polymer thick films, when combined with ferrite fillers, can withstand temperatures of up to 200°C or less, depending on the polymer matrix. This technique enables the production

of highly integrated power circuits, which is particularly valuable for compact and efficient designs. Ferrite particles, typically around 10 micrometres in size, are obtained through standard methods. More recently, a hatch-type micro-powder blasting process has been developed, allowing for the precise micro-structuring of ferrite cores from thin ferrite wafers, usually around 1 millimetre thick. These microstructure ferrite transformers are well-suited for low-power applications operating at frequencies up to 1 MHz

The losses in ferrites are influenced by several factors, including hysteresis loss at low frequencies, conductivity (or eddy current) loss, and relaxation-resonance loss at high frequencies, with their structure being quite complex. A model based on the Preisach theory has been applied to predict the hysteretic behaviour of soft ferrites, particularly for power electronics applications. This model has yielded good results, especially at low frequencies, helping to better understand and optimize ferrite performance in various power-related devices.

#### **1.4.3 Electromagnetic Interference (EMI) Suppression**

The significant increase in electronic devices such as high-speed digital interfaces in notebooks, digital cameras, computers, scanners, and similar devices, all operating in compact spaces, has greatly increased the likelihood of electromagnetic interference (EMI) affecting these systems. The rapid growth of wireless communications has further contributed to this issue, leading to interference induced by electric and magnetic fields. Electromagnetic interference is defined as the degradation in the performance of an electronic system due to external electromagnetic disturbances.

Noise from electronic devices is typically generated at frequencies higher than the operating frequencies of the circuits. To mitigate EMI, suppressors are used, which function as low-pass filters. These filters block signals with frequencies higher than a certain threshold, effectively minimizing the interference and protecting the integrity of the system's performance.

There are several approaches to building EMI suppressors, including the use of soft ferrites, ferromagnetic metals, encapsulated magnetic particles, ferromagnetic metal/hexaferrite composites, and carbon nanotube composites. Ferrite components, in particular, have been utilized for decades in EMI suppression applications. In recent years, the



demand for these materials has grown due to trends in miniaturization, increased integration density, and the rise in higher clock frequencies, especially in communication, computing, and information technologies.

Hexaferrites, in particular, have emerged as a remarkable alternative to cubic ferrites for EMI suppressor components. These materials offer higher resonance frequencies, comparatively high permeabilities at microwave frequencies, and greater electrical resistivities. These characteristics make hexaferrites an ideal choice for advanced EMI suppression in modern electronic systems.

Without the use of traditional magnetic materials, carbon nanotube-polystyrene foam composites have demonstrated significant EMI shielding effectiveness, primarily through the reflection of electromagnetic radiation. When combined with ferrite nanoparticles, carbon nanotubes can efficiently absorb microwave radiation. By using  $\text{CoFe}_2\text{O}_4$  nanoparticles as catalysts, a novel carbon nanotube/ $\text{CoFe}_2\text{O}_4$  spinel nano composite was created through a chemical vapor deposition method.

In the case of carbon nanotubes, dielectric loss plays a key role in the dissipation of electromagnetic wave energy, while the microwave absorption of pure Co ferrite is primarily associated with magnetic losses. However, each mechanism individually provides weak absorption. The true microwave absorption capability is enhanced when these two mechanisms are combined in a nanocomposite. The synergy between the two arises from a better alignment between magnetic loss and dielectric loss. This combination of ferromagnetic material ( $\text{CoFe}_2\text{O}_4$ ) and paramagnetic nanotubes leads to significantly improved microwave absorption performance, making the nanocomposite a much more efficient absorber.

#### 1.4.4 Biosciences

Magnetic materials, specifically nanoparticles like magnetite, are found in various living organisms and are used in a wide range of applications. While magnetic nanoparticles can be synthesized in the laboratory using well-established methods, biogenic magnetic particles, produced by living organisms, often exhibit superior properties compared to synthetic ones. These biogenic particles have a defined size range and width-to-length ratio, as well as high chemical purity. Additionally, they tend to have nearly perfect crystallographic structures

and may even display unusual crystallographic morphologies. The extracellular production of magnetite particles at the nanometres scale by various types of bacteria has been well-documented, highlighting their potential for use in various applications.

In some cases, biogenic magnetic particles are encapsulated by a lipid layer, which enhances their stability and makes them highly biocompatible. This characteristic has led to the development of many biotechnological applications based on both biogenic and synthetic magnetic micro- and nanoparticles. One notable application involves using magnetic nanoparticles to guide radionuclides to specific tissues. A new method has been developed to directly label a radioisotope with ferrite particles *in vivo*, specifically for liver tissue in rats.

These magnetic nanoparticles have therapeutic potential, especially when conjugated with other medical agents. Superparamagnetic magnetite particles can be selectively associated with healthy regions of tissues, such as the liver, during magnetic resonance imaging (MRI). In MRI, these particles alter the rate at which protons decay from the excited to the ground state, which results in a darker and distinct contrast for the healthy tissues.

In hyperthermia treatments—where specific tissues or organs are heated to treat cancer—thermal energy generated by hysteresis loss in ferrites can be used to target and heat the affected tissues, providing an effective therapeutic approach.

The temperature in tumour tissues can be elevated, making them more sensitive to radiation or chemotherapy. In addition to magnetite, several spinel ferrites and hexaferrites are also being researched for their potential in this area. A key technique in biotechnology involves using magnetic nanoparticles to bind enzymes, antibodies, oligonucleotides, and other biologically active compounds. These compounds can then be targeted to specific sites or removed from the system using an external magnetic field. Once targeted, these compounds can exert their effects on the designated tissue or serve as affinity ligands to target specific molecules or trap cells.

Magnetic nanoparticles have a wide range of applications, including the detection, modification, isolation, and study of cells, as well as the isolation of biologically active compounds. For modern electronic products like video cameras, cell phones, notebook computers, hard drives, and floppy drives, ferrites play a crucial and indispensable role as a primary component.

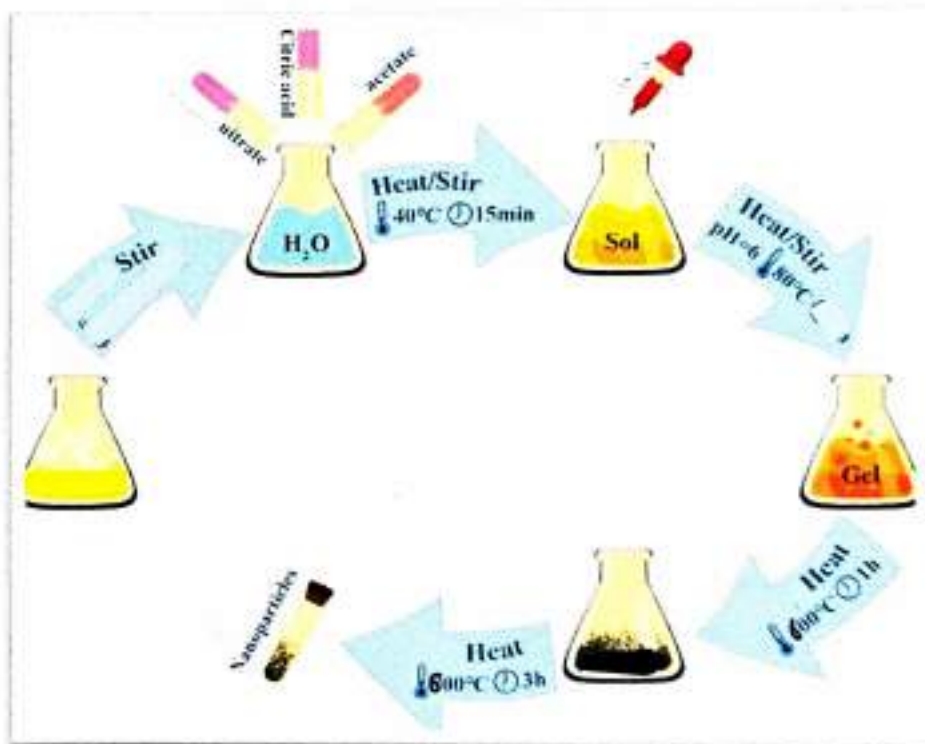
## Reference:

1. J. Smit and H. P. J. Wijn Ferrites (Philips Technical Library, Eindhoven, 1959).
2. R. Valenzuela Magnetic ceramics. Cambridge University Press, 1994.
3. F.S. Li, L. Wang, J.B. Wang, Q.G. Zhou, X.Z. Zhou, H.P. Kunkel, G. Williams, J. Magn. Mater. 268(2004) 332.
4. B. Viswanathan, V.R.K. Murthy: Ferrite Materials. Springer Verlag, Berlin (1990)
5. P. Vijaya Bhasker Reddy, B. Ramesh, Ch. Gopal Reddy, Physica B: Cond. Matter 405 (2010) 11.52.
6. Sagar E. Shirsath, B.G. Toksha, R.H. Kadam, S.M. Patange, D.R. Mane, Ganesh S. Jangam, Ali Ghasemi, J. Phys. Chem. Solids 71 (2010) 1669.
7. D. R. Mane, D. D. Birajdar, Swati Patil, Sagar E. Shirsath, R. H. Kadam, J. Sol-Gel Sci. Tech. (Published Online) DOI: 10.1007/s10971-010-2357-8.

## Chapter 2: Synthesis of $\text{Ni}_{1-x}\text{Mg}_x\text{Fe}_2\text{O}_4$

### Sol – gel Process :

The sol-gel process is a method used to create solid materials, particularly metal oxides, from a liquid sol (colloidal solution) that undergoes a chemical transformation into a gel. This process involves hydrolysis and polycondensation reactions, ultimately forming a network structure.





## Calculation -

- Molecular weight of Nickel = 58.693 g/mol
- Molecular weight of Magnesium = 24.305 g/mol
- Molecular weight of Ferrite = 55.645 g/mol
- Molecular weight of Oxygen = 15.999 g/mol

## Objectives –

To synthesize  $\text{Ni}_{1-x}\text{Mg}_x\text{Fe}_2\text{O}_4$  nanoparticles by sol-gel auto combustion reaction.







#### PHASE I

- Survey of Photocatalyst Nanomaterials based on sol-gel auto combustion method

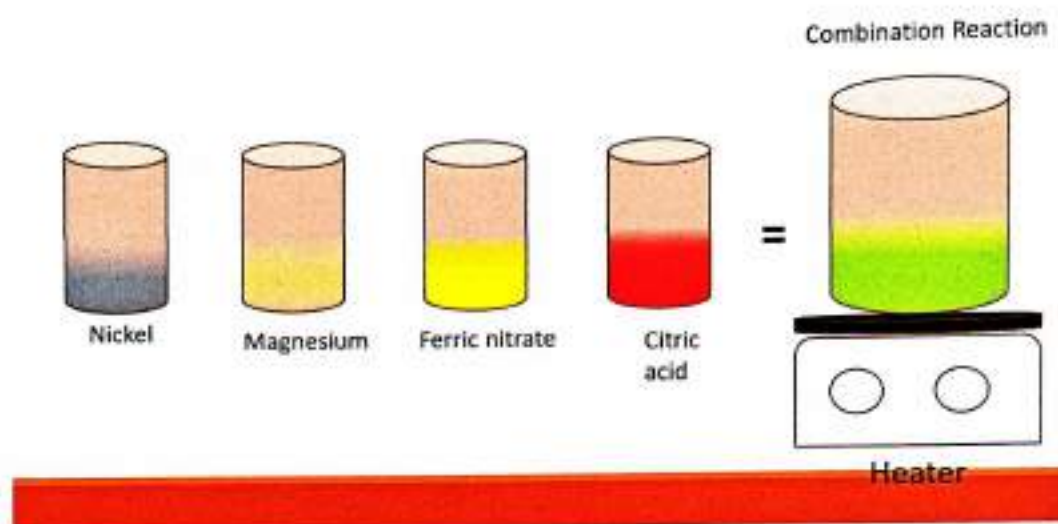
#### PHASE II

- Synthesis of  $\text{Ni}_{1-x}\text{Mg}_x\text{Fe}_2\text{O}_4$  by sol-gel auto combustion method

#### PHASE III

- Characterization of  $\text{Ni}_{1-x}\text{Mg}_x\text{Fe}_2\text{O}_4$  nanoparticles

## Synthesis of $\text{Ni}_{1-x}\text{Mg}_x\text{Fe}_2\text{O}_4$



### Preparation parameters –

x	Nickel Nitrate	Magnesium nitrate	Iron (III) nitrate	Citric acid	Fuel to oxidant ratio
0	0 gm	5.128 gm	8.08 gm	3.843 gm	1
0.2	1.163 gm 0.2 mole	4.103 gm	8.08 gm	5.337 gm	1
0.4	2.326 gm 0.2 mole	3.077 gm	8.08 gm	3.843 gm	1
0.6	3.489 gm 0.2 mole	2.051 gm	8.08 gm	3.843 gm	1
0.8	4.653 gm 0.2 mole	1.026 gm	8.08 gm	3.843 gm	1
1.0	5.128 gm	0 gm	8.08 gm	5.337 gm	1

### Chapter 3: Literature survey

A series of Magnesium substituted Nickel nano ferrites having the chemical formula  $Ni_xMg_{1-x}Fe_2O_4$  (where  $x = 0.0, 0.2, 0.4, 0.6, 0.8$  and  $1.0$ ) were prepared by Citrate Gel Auto-combustion method. The starting materials were Nickel Nitrate ( $Ni(NO_3)_2 \cdot 6H_2O$ ), Ferric Nitrate ( $Fe(NO_3)_3 \cdot 9H_2O$ ), Magnesium Nitrate ( $Mg(NO_3)_2 \cdot 6H_2O$ ), Citric acid ( $C_6H_8O_7 \cdot H_2O$ ) and Ammonia ( $NH_3$ ) all of 99% pure AR grade. Metal nitrates were employed in this process as they have a dual role of being a soluble cation sources and the oxidant [14]. Calculated quantities of metal nitrates were dissolved together in a minimum amount of distilled water to get clear solution. An aqueous solution of Citric Acid was then added to the metal nitrate solution. Citric acid was used with 2 important roles: the fuel for the combustion reaction and as a chelating agent to form complexes with metal ions, preventing the precipitation of hydroxylated compounds [15]. The molar ratio of Citric acid to the total moles of nitrate ions was adjusted to 1:3. The mixture was stirred to obtain a homogeneous solution and then was slowly

heated to  $80^\circ C$  at a rate of  $5^\circ C/minute$  using a hot plate magnetic stirrer. PH of the solution was adjusted to 7 by adding Ammonia ( $NH_3$ ) solution. A Sol is formed. The resulting solution was evaporated to dryness by heating at about  $150^\circ C$  on a hot plate with continuous stirring. As a result the viscosity rose due to cross linking of carboxylato-metal complexes into a three dimensional structure (pi-erre et al., 1990; Jang et al., 1995, Narebder abd Messing, 1997) and get started to form a viscous gel (Figure 1(a)). When finally all water molecules were removed from the mixture by increasing the temperature to  $200^\circ C$ , the viscous gel began frothing. The gel gave a fast flameless auto combustion reaction with the evolution of large amounts of gases (Figure 1(b)). It started in

the hottest zones (Figure 1(c)) of the beaker and propagated from the bottom to the top like the eruption of a Volcano (Figure 1(d)). The reaction was completed in a minute giving rise to dark grey voluminous product with a structure similar to Branched tree (Figure 1(e)). Finally the burnt powder was ground and was calcined in air at temperature 500°C for four hours to obtain a spinel phase.

Ferrites form a very good class of electrical materials because of their high resistivity and low loss behaviour, and hence have vast technological applications over a wide range of frequencies Ferrites are preferred in the field of electronics and telecommunication industry because of their novel electrical properties which makes them useful in radiofrequency circuits, high quality filters, rod antennas, transformer cores, read/write heads for high digital tapes and other devices. Hence it is important to study their dielectric behaviour at different frequencies. The dielectric properties of ferrites are dependent on several factors, such as method of preparation, heat treatment, sintering conditions, chemical composition, cation distribution and crystallite size [1].

Ferrites, a distinct class of magnetic materials known as ferromagnetic have spinel structure. They consist of spontaneously magnetized domains and show the phenomena of magnetic saturation and hysteresis. Spinel ferrites possess properties of both magnetic materials and insulators and are important in many technological applications. The interesting physical and magnetic properties of spinel ferrites arise from the ability of these compounds to distribute the cations among the available tetrahedral (A) and octahedral (B) sites [2]. Spinel ferrites have gained lot of attention because of their remarkably high electrical and magnetic flux induction. They are considered as good dielectric and are found in many technological applications. Increased application of ferrites has led to the development of many chemical methods which includes hydrothermal, co-precipitation and sol-gel for the preparation of stoichiometric and chemically pure spinel ferrites [3].



Nickel ferrites are known for high power handling capability at microwave frequencies due to their high curie temperature which makes other magnetic properties of this series relatively independent of temperature [4]. Nickel and Magnesium ferrite is extensively used in a number of electronic devices due to their high permeability at high frequency, remarkable high electrical resistivity, mechanical hardness, chemical stability and reasonable cost [5].  $\text{NiFe}_2\text{O}_4$  is a well known inverse spinel with  $\text{Ni}^{2+}$  at octahedral [B-site] and  $\text{Fe}^{3+}$  ions distributed equally in tetrahedral (A-site) and octahedral sites [B-site] [6]. Magnesium ferrite ( $\text{MgFe}_2\text{O}_4$ ) is one of the most important ferrites. It has a cubic structure of normal spinel-type and is a soft magnetic n-type semiconducting material, which finds a number of applications in heterogeneous catalysis, adsorption, sensors, and in magnetic technologies [7]. Recently, nanostructures of magnetic materials have received more and more attention due to their novel material properties that are significantly different from those of their bulk counterparts [8-12].

In this study, samples with the formula  $\text{Ni}_{1-x}\text{Mg}_x\text{Fe}_2\text{O}_4$  ( $x=0.0, 0.2, 0.4, 0.6, 0.8$  and  $1.0$ ) were synthesized via the Citrate gel Auto-Combustion method. The energy to form the ferrite nano-crystallites is provided by oxidation-reduction process of thermal precursor and fuel in the

the	Citrate	-Gel	auto-combustion	process
-----	---------	------	-----------------	---------



## Chapter 4: characterisation Technique

### 4.1. XRD

#### 4.1.1 Introduction

The characterization of deposited thin films is essential, especially for applications in supercapacitor devices. In this study, suitable techniques were utilized to analyse the physical properties of the thin films, including crystal structure, microstructural details, film composition, surface morphology, optical characteristics, chemical bonding configurations, and electrical properties, in order to optimize the deposition conditions.

#### 4.1.2 Structural Analysis

The crystallographic properties of thin films play a crucial role and significantly influence their physical characteristics, including atomic arrangement, electrical conductivity, carrier mobility, optical band gap, and electrical resistivity. These structural features are primarily determined by the film's chemical stoichiometry, the mode of operation, and deposition conditions. Understanding the structural properties of thin films is vital for research, process development, and ensuring device reliability. In this study, structural aspects such as crystalline phases, grain size, and preferred orientation of the films were thoroughly examined.

X-ray Diffraction (XRD) is one of the most commonly used techniques for analysing the crystallographic structure of thin films. It provides detailed information about lattice parameters, crystal structure, orientation, crystallite size, structural defects, and internal stresses present in the films. The fundamental principle of XRD is based on the diffraction of a collimated X-ray beam—typically with a wavelength between 0.5 and 2.0 Å—by the crystalline planes in the sample, in accordance with Bragg's law, which is expressed as

$$n\lambda = 2d \sin\theta$$

Where

$d$  is the spacing between atomic planes in the crystalline phase,

$\theta$  is the diffraction angle

$\lambda$  is wavelength of x rays

$n$  is the order of the diffraction

An X-ray diffraction system typically comprises an X-ray tube, a monochromator, and a detector, all aligned so that the focal point of the X-ray source, the center of the orientation system, and the centre of the detector aperture lie on a plane perpendicular to the  $2\theta$  axis. The system also includes a pulse counting scale connected to the detector. The wavelength of the X-rays is controlled using a combination of the characteristic emission line of the selected target material and the absorption edge of a specific filter material. To determine the structural composition of a sample, measurements are taken from multiple orientations to calculate the interplanar spacing, which is then compared with known values.

In the present study, a Seifert X-ray Diffractometer was used. The X-ray generator was operated at 40 kV and 30 mA. The X-ray source scanned the thin films over a  $2\theta$  range of  $20^\circ$  to  $70^\circ$ , with a scanning rate of  $0.5^\circ$  per minute. Interplanar spacing ( $d$ ) was calculated from the XRD data using Bragg's law.

The lattice planes ( $hkl$ ) of the deposited films were identified using standard JCPDS (Joint Committee on Powder Diffraction Standards) data. The lattice constants were then calculated using appropriate equations for a cubic crystal structure, where ( $hkl$ ) represents the Miller indices and  $a$  is the lattice constant.

The crystallite size ( $L$ ) of the films was estimated from the XRD peak broadening using Scherrer's equation:

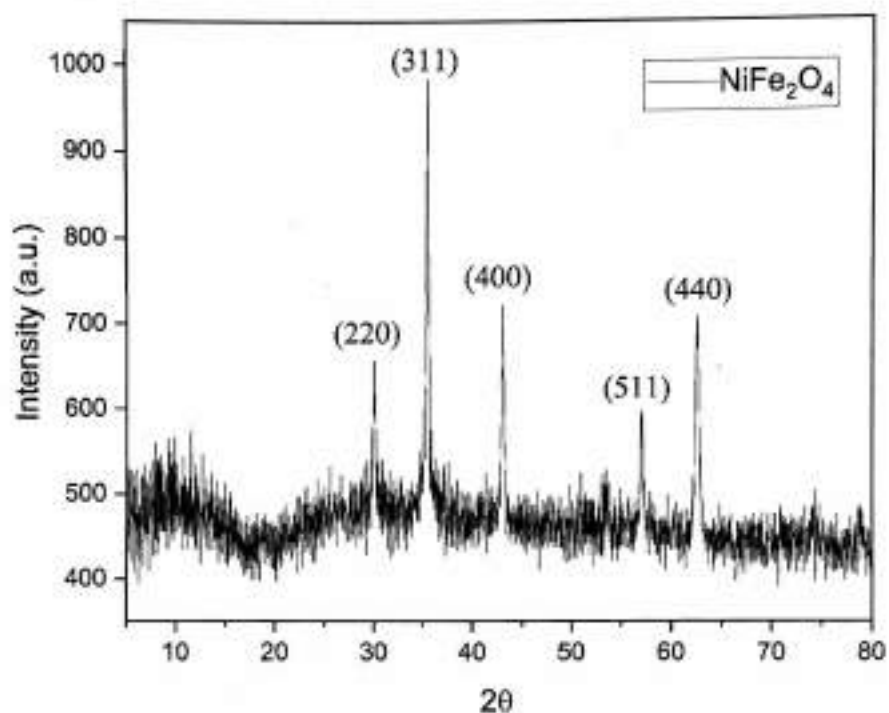


**Figure 1.** X-ray diffraction pattern of  $\text{NiFe}_2\text{O}_4$  annealed at  $600^\circ\text{C}$  for 2 h.

In order to research the crystal structure of prepared powder material XRD analysis was performed. The resultant XRD pattern is shown in figure 1.

The formation of cubic spinel structure is confirmed with the peaks (220), (311), (400), (511) and (440). No any secondary phase was observed confirming the lack of impurity. The XRD pattern matches well with the standard data (JCPDS card no. 86-2227).



## Chapter 5: Conclusion

### IV. Conclusions

Citrate Gel auto combustion technique is a convenient way for obtaining a homogeneous nano sized mixed Ni-Mg ferrites.

The process involves no impurity pickup and material loss. It is a very simple and economical method where no specific heating or cooling rate is required. It is a low temperature processing technique and requires shorter sintering duration.

X-ray diffraction pattern confirms the formation of cubic spinel structure in single phase without any impurity peak. It is in good agreement with the standard data from ICSD

The crystallite size of the various Ni-Mg ferrites was in the range of 16-36nm.

The lattice parameter is increased with the increase of Mg substitution in Ni-Mg ferrites which indicates that the mixed Ni-Mg ferrite system obeys Vegard's law.

SEM micrographs of various compositions indicate the morphology of the particles is similar. They reveal largely agglomerated, well defined nano particles of the sample powder with inhomogeneous broader grain size distribution.

EDS data gives the elemental% and atomic % in the mixed Ni-Mg nanoferrites and it shows the presence of Ni, Mg, Fe and O without precipitating cations.

#### References :

- [1] M. Abdullah Dar, Khalid MijasamBattoo, Vivek Verma, W.A. Siddiqui, R.K., "Synthesis and characterization of nano-sized pure and Al-doped lithium ferrite having high value of dielectric constant" Journal of Alloys and Compounds, 493.pp 553-560,2010.
- [2] K.H.Maria, S.Choudhary,M.A.Hakim "Complex Permeability and Transport Properties of Zn Substituted Cu ferrites", Journal of Bangladesh Academy of Sciences, Vol.34, Nol,pp1-8,2010.
- [3] M.H.Khedr., "Effect of firing temperature and compacting pressure on the magnetic and electrical properties properties of nickel ferrite", Journal of physicochemical problems of mineral processing, Vol 38,pp 311-320,2004.
- [4] N.S. Bhattacharyya, G.P.Srivatava, On the

# SYNTHESIS AND CHARACTERIZATION OF COPPER OXIDE THIN FILM BY SILAR METHOD

A Project Report Submitted To  
**VIVEKANAND COLLEGE, KOLHAPUR**

For The Partial Fulfillment

Of

Master of Science

In

**PHYSICS**

Under The Faculty of Science


By

Miss. Gouri Balasaheb Gavade

Under The Guidance Of

Dr. S.I. Inamdar madam

Professor, M.Sc ,Ph.D.

  
Teacher Incharge

Examiner

  
Head of department

**HEAD**  
DEPARTMENT OF PHYSICS  
VIVEKANAND COLLEGE, KOLHAPUR  
(EMPOWERED AUTONOMOUS)



## CERTIFICATE

This is to certify that the project entitled "Synthesis and characterization of Copper Oxide thin films by SILAR method" which is being submitted herewith for the award of the Degree of Master of Science in Physics of Vivekanand College, Kolhapur is the result of the original project work completed by Miss. Gouri Balasaheb Gavade under my supervision and guidance and to the best of my knowledge and belief the work embodied in this project has not formed earlier the basis for the award of any Degree or similar title of this or any other University or examining body.

Place: kolhapur

Date: 30/04/2025

*G. Gavade*  
Examiner

*S.S. Lathe*  
H.O.D  
(Dr. S.S. Lathe)

Project Guide

*S.I. Inamdar*  
Dr. S.I. Inamdar madam

Department of Physics, Vivekanand College, Kolhapur.

HEAD  
DEPARTMENT OF PHYSICS  
VIVEKANAND COLLEGE, KOLHAPUR  
(423 001, 423 002, 423 003, 423 004, 423 005)

# DECLARATION

I hereby declare that, the project method entitled "**Synthesis and characterization of copper oxide thin films by SILAR method**" completed and written by me has not previously formed the basis for the award of any Degree or Diploma or another similar title of this or any other University in India or any other country or examining body to the best of my knowledge.

Place: Kolhapur

Date: 30/04/2025



Miss. Gouri Balasaheb Gavade

M.Sc.I (Solid State Physics)

## ACKNOWLEDGEMENT

At the outset, I should like to express my deep felt gratitude and indebtedness to my guide Dr. S.I. Inamdar madam, Department of Physics, Vivekanand College, Kolhapur. Her unceasing encouragement, optimum vast experience and commitment towards research have left a deep impression on me; will stand in good stead in future also.

I express profound regard and gratitude to Prof. Dr. S.S.Latthe sir, Head of Department of Physics, Vivekanand College, Kolhapur, for making me available the laboratory facilities and for their kind support and co-operation in my work. I take this opportunity to thank to all our teachers in department for their kind co-operation throughout my study. I am also thankful to non-teaching staff of the department for their co-operation during our work. I am grateful to authorities and staff for their kind assistance and providing facilities and staff of Library for providing the necessary books, Journals and Internet facilities accessible to me.

I am at the loss of words while expressing my deep feelings of gratitude towards my family members, for support and inspiration which has sustained me through my life.

Place: Kolhapur

Date:30/04/2025



## MAIN INDEX

CHAPTER NO.	TITLE	PAGE NO.
I	Introduction	
II	Thin film deposition technique and characterization & theoretical background of SILAR method	
III	Result, Discussion & Conclusion, References	

# Chapter I

## Introduction

## Index

I.	Introduction	
II.	Chapter II	
III.	Chapter III	



## **INTRODUCTION:**

Metal oxides are important from both scientific and technological perspectives. They present interesting opportunities for research. Especially thin films offer opportunities to pursue structure property relations using controlled microstructures.

Copper oxide is known to exist in two semiconducting phases, namely cupric oxide ( $\text{CuO}$ ); and cuprous oxide ( $\text{Cu}_2\text{O}$ ). An intermediate compound between the previous two, a metastable copper oxide,  $\text{Cu}_2\text{O}_3$  has been also reported.  $\text{CuO}$  which has band gap between 1.4-2.1 eV, exhibits versatile range of applications. As a mineral, it is known as tenorite. It is a product of copper mining and the precursor to many other copper-containing products and chemical compounds.<sup>[3]</sup>

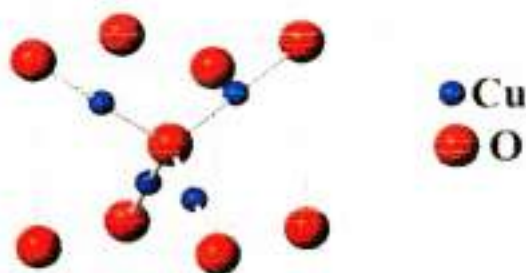
$\text{CuO}$  exhibits a range of potentially useful physical properties like superconductivity, high temperature, electron correlation effects, and spin dynamics. Cupric oxide may be found in over-the-counter vitamin-mineral supplements as a source of copper.

Both the structural and surface properties of  $\text{CuO}$  thin films were improved with the increase in the deposition cycles as a result of which the optical absorption edge of  $\text{CuO}$  shift towards longer wavelength, and the optical band gap energy decreases from 2.48 eV to 2.31 eV. The room temperature photoluminescence spectrum showed blue emission band centered at 468 nm, attributed to the near-band-edge emission of  $\text{CuO}$ .

## Properties of Copper Oxide(II):

Properties	
Chemical Formula	CuO
Molar Mass	79.545 g/mol
Appearance	Black to brown powder
Density	6.315g/cm <sup>3</sup>
Melting Point	1,326 °C (2,419 °F; 1,599 K)
Boiling Point	2,000 °C (3,630 °F; 2,270 K)
Solubility in water	insoluble
Band gap	1.2 eV
Magnetic susceptibility ( $\chi$ )	$+238.9 \cdot 10^{-6} \text{ cm}^3/\text{mol}$

### Crystal structure of copper oxide(II):



CuO crystallizes in a monoclinic structure with the lattice parameters of  $a=4.684 \text{ \AA}$ ,  $b=3.425 \text{ \AA}$ ,  $c=5.129 \text{ \AA}$  and  $\beta=99.28^\circ$ .

CuO thin film has transmittance of 20% in the visible spectrum and it could reach 90% for the high wavelength of the visible region with 2 to 2.5 refractive index value. CuO thin films were reported as p-type conductivity due to copper vacancies in the

structure. CuO is a promising semiconductor for solar cell fabrication, such as a solar absorber due to high solar absorbency and a low thermal emittance.

# Chapter II

**Thin film deposition technique and  
characterization & theoretical background of  
SILAR method**



## **Introduction:**

On account of two-dimensional solids potential, specialized qualities and logical interest in the properties, the field of thin films has turned out to be evergreen as of late. Until, adequate advance improvement has not been made to give sensible logical certainty to thin film inquire about. The helpfulness of the slender films and logical interest around two-dimensional solids have been in charge of the inundate enthusiasm for the investigation of the science and innovation of thin films. Thin films have been utilized in the investigation of the connection between the structure of solids and their physical properties. Practical applications incorporate electrical circuits, optical instruments and attractive data storing devices. Thickness of the thin film is generally examined as angstrom units ( $\text{\AA}$ ). Thin films are shaped by depositing material onto a clean supporting substrate to develop film thickness, as opposed to by weakening mass material. A surface limited between two parallel plane increasing interminably in two ways confined in the measurement along third direction.

Any strong or fluid framework has at most two-dimensional request or periodicity is called as thin film. The thin strong films were most likely previously acquired by electrolysis in 1838. The customary mass material is portrayed by three-dimensional request in which the comprise particles or atoms get themselves. This request or periodicity is in charge of the structure/idea of the material, which thus is at the core of particular physico-chemical properties of the materials. If there should be an occurrence of thin films, the framework has at most two-dimensional request or periodicity. This records for the immense distinction in physico-compound properties between bulk material and its thin film counterpart. Utilizations of thin film revolution in the field of optics, sensor, sensors, energy storage device (supercapacitor) and magnetism. The requirement for better than ever optics, sensor and attractive devices has strengthened the

investigation of thin solid films of components just as parallel and ternary structures, with controlled organization and explicit properties [1].

### **Physical properties of thin film-**

The mechanical properties of thin films are very unique in relation to those of the mass material for example the qualities shown by a few films give off an impression of being as much as multiple times as extraordinary concerning all around strengthened mass examples and are generally a few times as incredible as the qualities of extremely cold worked mass material. An electronic impact of slenderness is seen in thin dielectric films as an unexpected change in the conductance at steady field as the thickness is decreased below some limited measurement. With dielectric films thicker than about  $100\text{\AA}$ , the field required to make a given flow stream is commonly free of film thickness. More slender films, anyway show a large increment in current thickness due to "burrowing". This is on the grounds that the likelihood of an electron with a given vitality entering the potential boundary introduced by the dielectric increments exponentially with reducing thickness. Thinness results likewise in a stamped change in the conductivity of metallic films as film thickness is the fate of indistinguishable request from, or littler than the electron mean free path. At the point when this happens dispersing of electrons at the film surface turns into a critical factor and the compelling conductivity is decreased. Perceptions of film resistivity as a component of thickness hence give one methods for evaluating the electron mean free path.

This technique has been discovered diverse by and by, since films of a high level of purity are required. The resistivity of metal films might be isolated into warm movement and another brought about by dissipating at cross section flaws. The blemishes in deposited metal films result in resistivity higher than those watched



for mass metals. The impact of temperature on the two methods of scattering isn't the equivalent and this outcome in contrasts between the temperature coefficients of opposition of mass metals and those of polycrystalline metallic films. The extent of this distinction might be utilized to construe the level of blemish in films.

The developing innovation needs different sorts of thin films for assortment of uses. Numerous materials have been set up as thin films over a century as a result of their potential specialized esteem and logical interest in their properties. Thin film is characterized, as any strong or fluid framework has just about 2-D request or periodicity. Properties of thin film vary altogether from those of mass to surface and interface impacts; this commands by and large conduct of the thin films. Thin films have wide scope of utilizations and reach out from the micrometer specks in microelectronic, photoelectronic, thermoelectronic, superconductivity, data storing media, energy 21 units, and bio-good coatings. The properties of thin films rely upon the technique for method. The required properties and flexibility can be acquired by picking appropriate technique for thin films method. Thin film deposition techniques can be extensively substitute either physical or chemical [2-3]. Under physical techniques, we have vacuum vanishing, and sputtering, where the deposition happens after the material to be kept has been exchanged to a vaporous state either by evaporation or an effect procedure. Under material techniques, we have the gas stage chemical procedures, for example, ordinary chemical vapor deposition (CVD), laser CVD, photograph CVD, metal organo-compound vapor deposition (MOCVD), and plasma upgraded CVD. Fluid stage chemical techniques incorporate electrodeposition, chemical bath deposition (CBD), material spray pyrolysis (M-CBD), progressive ionic layer adsorption and reaction (SILAR), electroless method, anodization, splash pyrolysis, fluid stage epitaxy, and so on. This part portrays the different techniques for thin film arrangement and different characterization systems

used to consider the properties of Nickel oxide thin films. The semiconducting material, in thin film structure are quite compelling of photovoltaic devices, transparent cathodes, surface acoustic wave devices, low emissivity covering for engineering glass, sun based front board show, different gas sensors, heat reflectors for cutting edge looking in sun based applications. Hence it is important to portray Nickel oxide thin films with different exploratory methods so as to get to the extent of further enhancement [4-5].

### **Methods of thin film preparation-**

In general, many thin film deposition techniques have one common element i.e. they are atomistic in character. In other words, they are grown one atom at a time. This enables the researchers to create thin film systems, which could not ordinarily be expected to be possible. To be able to fully exploit this, one requires good knowledge and appreciation of surface process as well as nucleation, growth and morphology of evolving films. Among all these techniques, most of the physical methods are cost expensive. There are two methods of thin film preparation as follows:

#### **Physical Vapor Deposition:**

Physical vapor deposition (PVD) is one of the vacuum coating processes in which the film of coating material is usually deposited atom by atom on a substrate by condensation from the vapor phase to the solid phase. It is widely used technique for the fabrication of thin films and surface coatings. PVD has been used a lot at the industrial scale and also has been combined with different methods to produce coatings with superior properties. Recent developments in nanoscience have made this technique more and more useful for the fabrication of layers with desired microstructure and properties. The most common physical vapor deposition methods are vacuum evaporation and sputtering. The procedure for physical vapor deposition is as follows: (i) sputtering/ evaporation of different components to produce a vapor phase; (ii) supersaturation of the



vapor phase in an inert atmosphere to promote the condensation of metal nanoparticles; (iii) consolidation of the nanocomposite by thermal treatment under inert atmosphere.

### **Chemical Vapor Deposition:**

Chemical vapor deposition (CVD) is used widely in materials processing technology. The majority of its applications involve applying solid thin-film coatings to surfaces, but it is used also to produce high purity bulk materials and powders, as well as fabricate composites. Chemical vapor deposition has been used to deposit a wide range of materials in many different areas. Chemical vapor deposition is a process in which the substrate is exposed to one or more volatile precursors, which react and/or decompose on the substrate surface to produce the desired thin film deposit. It is a method which is not restricted to a line-of-sight deposition which is a general characteristic of sputtering, evaporation, and other PVD processes. As such, CVD has high throwing power. The CVD includes different methods as follows:

SILAR Method

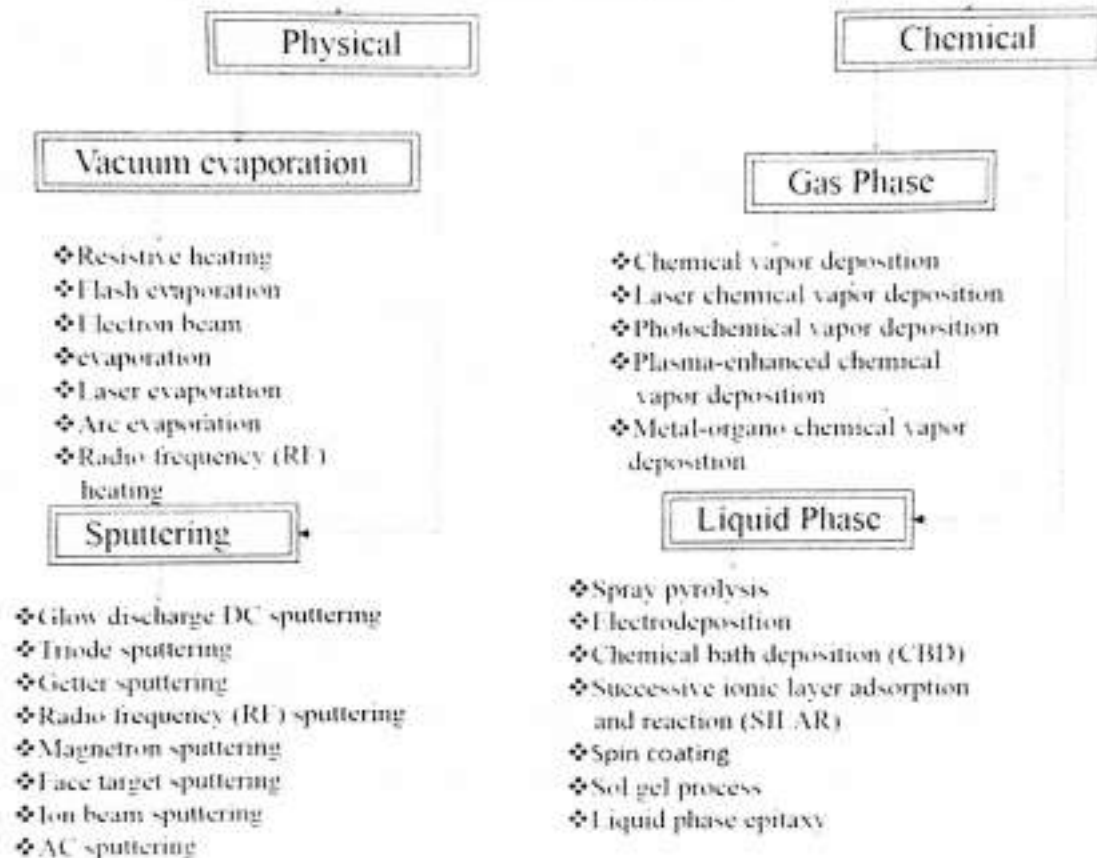
Spray Pyrolysis

Chemical Bath Deposition

Spin Coating

Sol gel method

## Thin Film Deposition Methods



### Thin Film Characterization Methods –

The properties of the films can be best understood using different characterization techniques. X-ray diffraction (XRD), scanning electron microscopy (SEM) were utilized in the present study. Different techniques used in the present study with their utility to find out different properties are summarized in Table and highlights are given below.

**Summary of different characterization techniques used in the present study to find properties of the films:**

Sr. No.	Characterization techniques	Thin film properties
1.	X-ray diffraction	Identification of material, crystal structure, crystallite size determination
2.	UV-VIS spectroscopy	Optical band gap
3.	Scanning electron microscopy (SEM)	Surface morphology
4.	FT-IR spectroscopy	To analyse functional group in the given sample

### **X-Ray Diffraction:**

X-ray diffraction (XRD) is ground-breaking trial system to get the data of organization, stage and crystallite introductions of the material precious stone structure, crystallinity, porosity and cross section parameters, which depend on the elucidation of the X-ray diffraction designs utilizing Bragg's law [6]. Enhanced discovery techniques for X-ray, the accessibility of commercial monochromators and intense micrococcus X-ray sources have made X-ray diffraction technique pertinent to films as thin as 100 °A. The few laborers have portrayed X-ray diffraction course of action, fit to the investigation of thin films. This method utilizes a chromator to give a diffracted bar, which is additionally diffracted from the film surface swaying about the mean diffraction position. The X-ray diffraction procedure dependent on monochromatic radiation is progressively critical in light of the fact that the dispersing of the planes (d-separating) can be found from the watched diffraction points. The marvel of X-ray diffraction can be considered as



impression of X-rays from the crystallographic planes of the material and is administered by the Bragg's condition

$$2d\sin \theta = n \lambda$$

Where 'd' is grid dispersing,  $\lambda$  is the wavelength of the monochromatic X-ray; 'n' is structure of diffraction and  $\theta$  is diffraction edge. The 'd' values are determined utilizing above connection for known estimations of  $\theta$ ,  $\lambda$  and n. The X-ray diffraction information in this way acquired is contrasted and American Standard for Testing for Materials (ASTM) to distinguish the obscure material. For thin films, the powder diffraction system related to diffractometer is most regularly utilized. Powder diffraction technique is first created by Debye and Scherrer [7] and A. W. Hull [8] Structure freely. The precious stone structure examination should be possible by X-ray diffractometer. A versatile counter in X-ray diffractometer replaces Debye Scherrer camera. The diffractometer essentially utilizes monochromatic radiations and can be put to research single or polycrystalline precious stone. Further, X-ray diffraction technique can be utilized to recognize crystalline materials from nanocrystalline (indistinct) materials. The structure ID is produced using the x-ray diffraction design investigation and contrasting it and the globally perceived database containing the reference design (JCPDS).

From X-ray diffraction design we can acquire the accompanying data:- (I) To pass judgment on arrangement of a specific material framework.

(II) Unit cell structure, cross section parameters, and mill operator records.

(III) Types of stages present in the material

(IV) Estimation of crystalline/formless material in the example.

(V) Evaluation of the normal crystalline size from the width of the crest in a specific stage design. Expansive precious stone size offers ascend to sharp peaks, while the peak width increases with decreasing crystal size.



(VI) An investigation of auxiliary mutilation emerging because of variety in d-dispersing brought about by the strain, warm contortion.

#### Determination of crystal size:

The X-ray diffraction investigation has been the most mainstream technique for the estimation of crystallite size in nanomaterials and along these lines, has been broadly utilized in the present work. The assessment of crystallite sizes in the nanometres run warrants cautious scientific aptitudes. The increasing of the Bragg crests is credited to the advancement of the crystallite refinement and inward stain. To estimate increasing and recolor widening, the full width at half most extreme (FWHM) of the Bragg crests as an element of the diffraction edge is investigated. Crystallite size of the stores is determined by the X-ray diffraction (XRD) peak increasing. Scanning Electron Microscopy (SEM) Scanning electron microscopy is utilized for assessing geographies of example at exceptionally high amplifications utilizing bit of hardware called checking electron magnifying instrument. SEM amplifications can go to more than 30000x. Be that as it may, a few semiconductors producing applications require amplification under 300x as it were. SEM investigation is frequently utilized in the examination of bite the dust/bundle breaks and facture surfaces, bond disappointments and physical imperfections on the bite the dust or bundle surface. To create the SEM picture, the electron bar is cleared over the region being investigated, delivering numerous signs. Amid SEM review, a light emission is centered on the spot volume of the example, bringing about the exchange of vitality to the spot. These besieging electrons, likewise alluded to as essential electrons, remove electrons from the example itself. The ousted electrons, otherwise called auxiliary electrons are pulled in and collected by an emphatically one-sided network or authority and moved into flag. These signs are then intensified, examined and converted into pictures of the geology being reviewed. At long last

the picture is appeared on a cathode ray tube (CRT) or some other showcase gadget. The SEM is utilized essentially for the examination of thick (for example electron dark) examples.

Electrons which are radiated or back dissipated from the example are gathered to give:

(1) Topological data (for example itemized state of example surface) if the low vitality optional electrons (not exactly or equivalents to 50 eV) are gathered,

(2) Nuclear number or introduction data if the high-vitality back dispersed electrons are utilized or if the spillage current to earth is utilized.

Imaging of attractive examples utilizing auxiliary and additionally back-dissipated electrons uncovers attractive area differentiate. Furthermore, two different signs can be gathered; the electron bar initiated present and light cathodoluminescence. The assembly edge of the test at the example is constrained by the diameter of the last gap and this point decides the profundity of field of a SEM. In this way the extensive profundity of field that is regularly connected with SEM pictures is in reality because of little combination point at the example, which is a lot smaller than the relating edge in optical magnifying lens. An extremely expansive estimation of profundity of field for high-goals picture, which underlines the estimation of high amplification SEM pictures of unpleasant surfaces.

### **UV- VIS Spectrophotometer -**

The term "band gap" refers to the energy difference between the top of the valence band and the bottom of the conduction band; electrons are able to jump from one band to another. In order for an electron to jump from a valence band to a conduction band, it requires a specific minimum amount of energy for the transition. The required energy differs with different materials. Electrons can



gain enough energy to jump to the conduction band by absorbing either a phonon (heat) or a photon (light). A material with a small but non zero band gap is referred to as a semiconductor. A material with a large band gap is called an insulator. In conductors, the valence and conduction bands may overlap, so they may not have a band gap. Bright and obvious (UV-Vis) retention spectroscopy is the estimation of the weakening of a light emission after it goes through an example or after reflection from an example surface. Retention estimations can be at a solitary wavelength or over an all-inclusive phantom range. Bright and obvious light are sufficiently fiery to elevate external electrons to higher vitality levels, and UV-Vis spectroscopy is normally connected to particles or inorganic buildings in arrangement. Fig indicates schematic of a solitary shaft UV-Vis spectrophotometer. The photons episode on any material might be reflected(R), transmitted (T) or retained (A). The amount of radiation of wavelength  $\lambda$  consumed by a material piece of thickness  $t$  is estimated regarding optical thickness ( $\alpha t$ ). Expecting unimportant reflection ( $R=0$ ), the vitality consumed can be given by Lambert's condition,

$$I = I_0 \exp(-\alpha t)$$

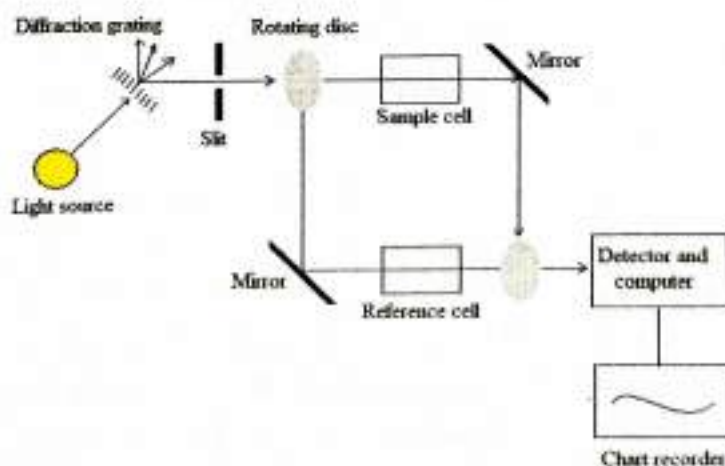


**Fig: Schematic of a single-beam UV-Vis spectrophotometer**

Where,  $I_0$  and  $I$  - incident and transmitted intensities respectively.  
In other words, optical absorption coefficient of films is evaluated from transmittance as,

$$T = A \exp(-\alpha t)$$

Where,  $T$  - Transmittance

$t$  - Film thickness

$A$  - Coefficient related to the refractive index, which is nearly equal to unity

$\alpha t$  - absorption coefficient.

A photon ingestion by a material is described by methods for electron change between vitality states or groups as indicated by quantum rules. A perfect semiconductor, at moderate temperature has modest number of openings in the valance band electrons in the conduction band. Assimilation of photons of adequate vitality will in general exchange the electrons from valance band to conduction band giving ingestion maxima. In this way, the optical assimilation edge at a specific occurrence photon vitality, which can be ascribed to the excitation of electrons structure valance to conduction band isolated by vitality equivalent to the band gap vitality ( $E_g$ ).

A well-focused mono-energetic ( $\sim 25\text{KeV}$ ) beam is incident on a solid surface giving various signals as mentioned above. Back scattered electrons and secondary electrons are particularly relevant for SEM application, their intensity being dependent on the atomic number of the host atoms. Each may be collected, amplified and utilized to control the brightness of the spot on a cathode ray tube. To obtain signals from an area, the electron beam is scanned over the specimen surface by two pairs of electro-magnetic deflection coils and so the C.R.T. ray in synchronization with this. The signals are transferred from point to point and signal map of the scanned area is displayed on a long persistent phosphor C.R.T. screen.



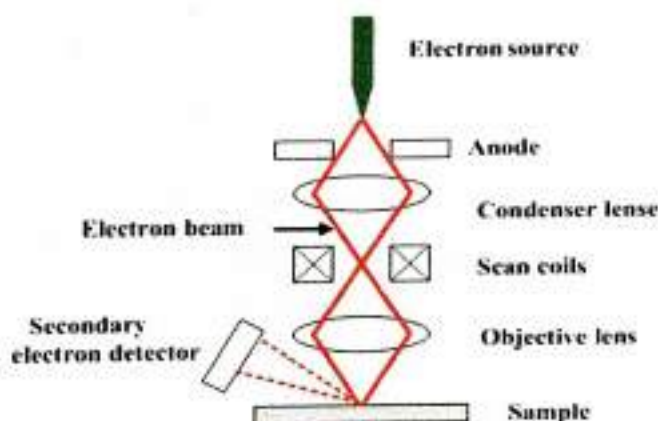
Change in brightness represents change of a particular property within the scanned area of the specimen.

### **Scanning Electron Microscopy (SEM)-**

Scanning electron microscopy is used for inspecting topographies of specimen at very high magnifications using piece of equipment called scanning electron microscope. SEM magnifications can go to more than 30000x. But some semiconductors manufacturing applications require magnification less than 300x only. SEM inspection is often used in the analysis of die/package cracks and fracture surfaces, bond failures and physical defects on the die or package surface. To produce the SEM image, the electron ray is swept across the area being inspected, producing many signals. During SEM inspection, a beam of electrons is focused on the spot volume of the specimen, resulting in the transfer of energy to the spot. These bombarding electrons, also referred to as primary electrons, dislodge electrons from the specimen itself. The dislodged electrons, also known as secondary electrons are attracted and collected by a positively biased grid or collector and transferred into signal. These signals are then amplified, analysed and translated into images of the topography being inspected. Finally the image is shown on a cathode ray tube (CRT) or any other display device. The SEM is used primarily for the examination of thick (i.e. electron opaque) samples. Electrons which are emitted or back scattered from the specimen are collected to provide: (1) Topological information (i.e. detailed shape of specimen surface) if the low energy secondary electrons (less than or equals to 50 eV) are collected, (2) atomic number or orientation information if the high-energy back scattered electrons are used or if the leakage current to earth is used.

Imaging of magnetic samples using secondary and or back-scattered electrons reveals magnetic domain contrast. In addition, two other signals can be collected; the electron beam induced

current and light cathodoluminescence. The convergence angle of the probe at the specimen is controlled by the diameter of the final aperture and this angle determines the depth of field of an SEM. Thus the large depth of field that is commonly associated with SEM images is in fact due to small convergence angle at the specimen, which is much smaller than the corresponding angle in optical microscopes. A very large value of depth of field for high-resolution image, which underlines the value of high magnification SEM images of rough surfaces.



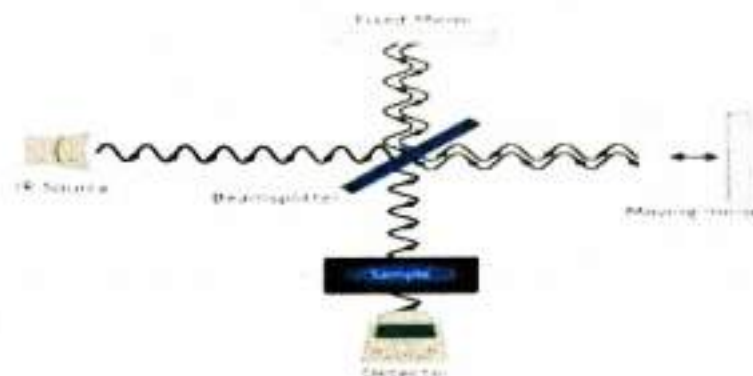
**Mechanism of SEM**

### **FT-IR Spectroscopy:**

Fourier Transform Infrared Spectroscopy is concerned with the vibration of molecule. Each functional group has its own discrete vibrational energy which can be used to identify the molecule through the combination of all the functional groups. The term fourier transform infrared spectroscopy originates from the fact that a fourier transform (a mathematical process) is required to convert raw data into the actual spectrum.

FT-IR spectroscopy is an analytical technique used to identify organic, polymeric and in some cases inorganic materials. The FT-IR analysis method uses infrared light to scan test samples and observed chemical properties.





## Working Mechanism of FT-IR

FT-IR analysis measures the range of wavelengths in the infrared region that are absorbed by a material. This is accomplished through the application of infrared radiation to samples of the material. The samples ability to absorb the infrared lights energy at various wavelength is measured to determine the materials molecular composition and structure. Unknown material are identified by searching the spectrum against a database of reference spectra. Materials can be quantified using the FT-IR material characterization technique as long as a standard curve of known concentrations of the component of interests can be created. A simple device called an interferometer is used to identify samples by producing an optical signal with all the IR frequencies encoded into it. Then, the signal is decoded by applying a mathematical technique known as fourier transformation. This computer generated process then produces a mapping of the spectrum information. The resulting graph is the spectrum which is then searched again reference libraries for identification.

With the microscope attachment samples as small as 20 microns can be analysed. This allows quick and cost effective identification of unknown particles, residues, films or fibres. FT-IR testing can also measure levels of oxidation in some polymers as well as quantifying contaminants or additives in materials.

## **Introduction:**

Copper oxides are relatively cheap, and stable in regard to their chemical and physical properties. It shows good photocatalytic activity. The potential application of CuO as anti-infective agents lies in their extremely high surface area and desirable crystal morphologies.

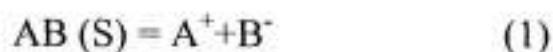
CuO which has band gap between 1.4-2.1 eV, exhibits versatile range of applications. As a mineral, it is known as tenorite. It is a product of copper mining and the precursor to many other copper-containing products and chemical compounds.

CuO exhibits a range of potentially useful physical properties like superconductivity, high temperature, electron correlation effects, and spin dynamics. Cupric oxide may be found in over-the-counter vitamin-mineral supplements as a source of copper.

There are different methods to utilize thin film of copper oxides.

## **Concept of solubility and Ionic product:**

Sparingly soluble salt AB, when placed in water, a saturated solution containing  $A^+$  and  $B^-$  ions in contact with undissolved solid AB is obtained and equilibrium is established between the solid phase and ions in the solution as



Applying law of mass action to this equilibrium,

$$K = C_A^+ + C_B^- / C_{AB} (S) \quad (2)$$

Where,  $C_A^+$ ,  $C_B^-$  and  $C_{AB}$  are concentrations of  $A^+$ ,  $B^-$  and AB in the solution respectively.

The concentration of a pure solid phase is a constant number i.e.

$$C_{AB} (S) = \text{constant} = K'$$

$$K = C_A^+ + C_B^- / K'$$



Or

$$KK' = C_A^{+} + C_B^{-} \quad (4)$$

Since K and K' are constant, the product KK' is also constant, say K<sub>s</sub>, therefore equation (4) becomes,

$$(5) \quad K_S = C_A^{+} + C_B^{-}$$

K<sub>s</sub> is called solubility product (SP) and  $(C_A^{+} + C_B^{-})$  is called as the ionic product (IP). When the solution is saturated, the ionic product is equal to the solubility product. But when IP exceeds the SP i.e.  $IP/SP = S > 1$ , the solution is supersaturated, precipitation occurs and ions combine on the substrate and in the solution to form nuclei. Solubility product is affected by temperature, solvent and particle size.

### **Theoretical background of SILAR Method:**

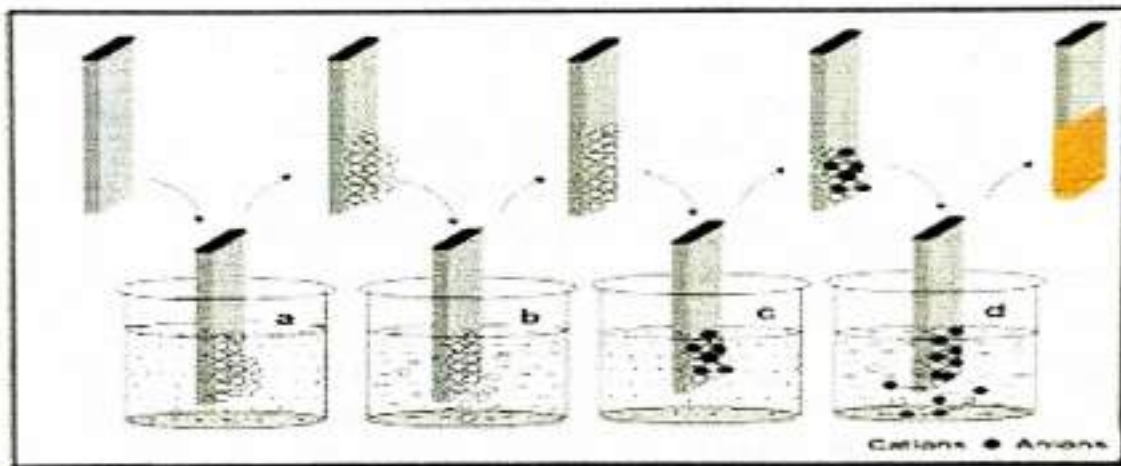
SILAR method mainly based on the adsorption and the reaction of the ions. From the solution and rinsing between every immersion with distilled water to avoid homogeneous precipitation of solution. The conservation of substance on the surface of another substance is known as adsorption, which is the fundamental building block of the SILAR method. The term adsorption can be defined as the interfacial layer between two phase of the system. Adsorption may be expected when two heterogeneous phases are brought into contact with each other. Hence, gas solid, liquid solid and gas liquid are three possible adsorption systems.

In SILAR method, we are concerned with adsorption in liquid solid system. Adsorption is an exothermic process. The adsorption is a surface phenomenon between ions and surface of substrate and is possible due to attraction force between ions in the solution and surface of the substrate. These force may be cohesive or wandaal's force or chemical attractive force. Atoms or molecules of substrate surface are not surrounded by atoms or molecules of their kind on all sides. Therefore, they possess unbalanced or residual force and hold the substrate particles. Thus, atoms can be holding on the substrate. The factors like temperature of solution, pressure,

nature of substrate, concentration of solution, area of the substrate, etc. affect the adsorption process. The reaction in pre-adsorbed (cations) and newly adsorbed (anions) forms a thin films of desired material.

It consists of at least four different steps:

1. Adsorption
2. Rinsing (I)
3. Reaction
4. Rinsing (II)



### Mechanism of SILAR method

#### Adsorption:

In this first step of SILAR process, the cations present in the precursor solution are adsorbed on the surface of the substrate and form the Helmholtz electric double layer. This layer is composed of two layers: the inner (positively charged) and outer (negatively charged) layers. The positive layer consists of the cations and the negative form the counter ions of the cations.

#### Rinsing (I):

In this step, excess adsorbed ions, are rinsed away from the diffusion layer. This results into saturated electrical double layer.



### Reaction:

In this reaction step, the anions from anionic precursor solution are introduced to the system. Due to the low stability of the material, a solid substance is formed on the interface. This process involves the reaction of surface species with the anionic precursor.

### Rinsing (II):

In last step of a SILAR cycle, the excess and unreacted species and the reaction byproduct from the diffusion layer are removed.

By repeating these cycles, a thin layer of material can be grown. Following the above-mentioned steps the maximum increase in film thickness per one reaction cycle is theoretically one monolayer. This results into a solid layer of the compound. Dividing the measured overall film thickness by number of reaction cycles, growth rate can be determined. This gives a numerical value for growth rate under the given conditions. If the measured growth rate exceeds the lattice constant of the material, a homogeneous precipitation in the solution could have taken place.

In practice, however, the thickness increase is typically less than or greater than a monolayer. Thus, the process involves an alternate immersion of the substrate in a solution containing a soluble salt of the cation of the compound to be grown. The substrate supporting the growing film is rinsed in highly purified deionized water after each immersion. The facts affecting the growth phenomena are the quality of the precursor solutions, their pH values, concentrations, counter ions, individual rinsing and dipping times. In addition, complexing agent and pretreatment of the substrate have been shown to affect the SILAR growth.

### SILAR deposition systems:

The critical operations for the deposition of thin films by successive ionic layer adsorption and reaction (SILAR) method, are adsorption of the cations, rinsing with deionized water, reaction of pre-adsorbed cations with newly adsorbed anions and again rinsing with



deionized water. Generally, manual, electropneumatic and computer based systems have been used to perform these operations in SILAR method. These methods are discussed in brief in the following sections.

- Manually operated:

This system does not require any power supply for operations, hence it is economical. In this system, four or more glass beakers of typically 50 ml capacity containing precursor solutions and deionized water are placed separately in the tray. The beakers containing precursor solutions and deionized water are alternately placed. The beaker containing deionized water is placed in between the beakers containing cationic and anionic precursor solutions. The immersion and rinsing of substrates are done manually. The SILAR deposition of sufficiently thick film requires many hours and therefore manual deposition of certain materials is not possible for a single person.

- Computer based:

The equipment consists of two beakers of 50 ml each containing the precursor solution and two rinsing vessels, lying in a circle on the circular tray. Each rinsing vessel being placed in between beakers containing cationic and anionic precursor solutions. The substrates are attached vertically by means of four arms. The arms are set out in line or a right angle and supported on the spindle. The spindle can turn and slide tightly in a bearing. Two stepping motors drive it. The computer program governs the vertical and translation movement of the spindle.

### **Experimental Details:**

In thin film deposition process, substrate cleaning is an essential factor to get reproducible films as it influences the smoothness, uniformity, adherence and porosity of the films. The substrate cleaning process relies on the nature of the substrate. The normal contaminants are oil, adsorbed water, air born dust, lint, oil particles, and so forth.

### **Substrate Cleaning:**

The following process has been adopted for cleaning the substrates.

- 1) The substrates were washed with detergent solution 'Labolene' and then with water.
- 2) These substrates were then cleaned with distilled water.
- 3) Then substrates were boiled in 0.5M chromic acid for about 1 hour.
- 4) Further substrates were cleaned with distilled water.
- 5) Then substrates were kept in ultrasonic cleaner for 15 minutes.
- 6) Then finally substrates were dried using dryer.

### **Preparation of solution:**

To prepare CuO thin films onto glass substrates a SILAR method was used.

#### **Solution 1:**

Cationic precursor solution was prepared by mixing (0.1 M) of copper (II) sulfate pentahydrate ( $\text{CuSO}_4 \cdot 5\text{H}_2\text{O}$ ) in 25 ml of water with constant magnetic stirrer for 5 min. After dissolving copper sulfate completely in water, aqueous solution of (0.1 M) of sodium thiosulfate was added. Sodium thiosulfate was added in aqueous solution of  $\text{CuSO}_4 \cdot 5\text{H}_2\text{O}$  until the solution become colorless with constant magnetic stirrer. The formation of colorless solution by adding sodium thiosulfate aqueous solution in  $\text{CuSO}_4 \cdot 5\text{H}_2\text{O}$  after constant stirring for 30 minutes.

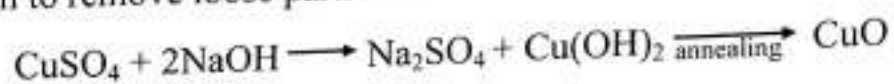
#### **Solution 2:**

Anionic precursor solution was prepared by dissolving sodium hydroxide of (0.1 M) in water with constant magnetic stirrer until it gets completely dissolved.

#### **Fabrication of thin film:**

For fabrication of CuO thin film well cleaned glass substrate was inserted in to the cationic precursor solution of ( $\text{CuSO}_4$ ,

$\text{Na}_2\text{S}_2\text{O}_3$ ) for 20s immersion in cationic precursor solution and rinsed in distilled water for 10s. The substrate was then immersed in the anionic precursor solution of (NaOH) that was kept under room temperatures for 20s and then also rinsed in distilled water again to remove loose particles.





# Chapter III

## Result, Discussion and Conclusion

## Result, discussion and conclusion –

### XRD-

To investigate the crystal structure CuO thin film configuration for XRD was used. In fig. shows pattern of XRD for resulting CuO sample fabricated. The main peaks that can be observed including (020), (021), (110), (002), (111), (113) phase orientation. The strong peak is 021 peak indicate that CuO material.

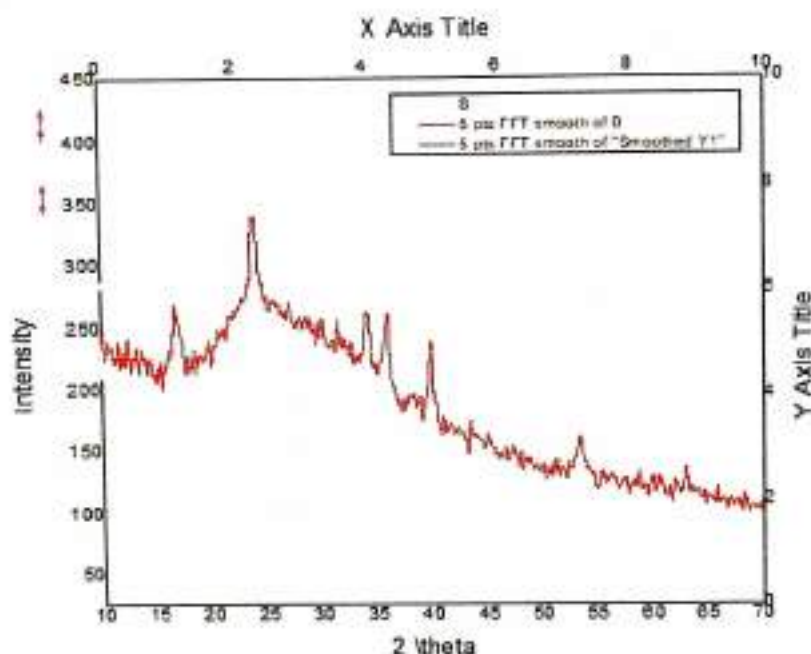


Fig. a) XRD peak pattern

### FT-IR –

The formation of single phase CuO was further confirmed by FTIR spectroscopy. Fig. b shows the FTIR spectrum of CuO nanocrystalline thin films deposition. All the films exhibit peaks between  $436\text{ cm}^{-1}$  and  $677\text{ cm}^{-1}$  which corresponds to the characteristic stretching vibrations of Cu–O bond in the monoclinic

crystal structure of CuO. FTIR result showed stretching of Cu-O bond are as expected. The peak corresponding to  $3500\text{cm}^{-1}$  shows the presence of O-H bond. This indicates trace amount of  $\text{Cu}(\text{OH})_2$  is present in the sample.

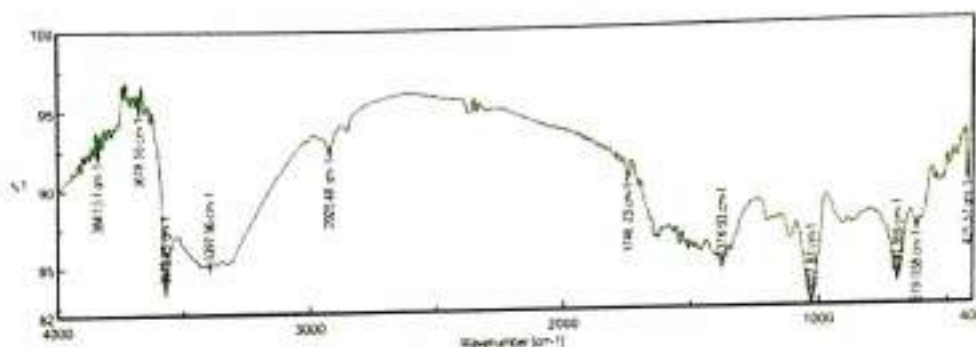


Fig.b) FT-IR peak pattern

## UV-VIS –

The UV-VIS absorption spectrum of CuO nanoparticles shows a strong blue shift compared to that of bulk. Band gap energy for thickness of 30 nm is 1.25 eV (fig.c), this matches with the indirect band gap value of CuO material. For thickness of 1.2nm, band gap of 1.55eV is observed (fig. d).



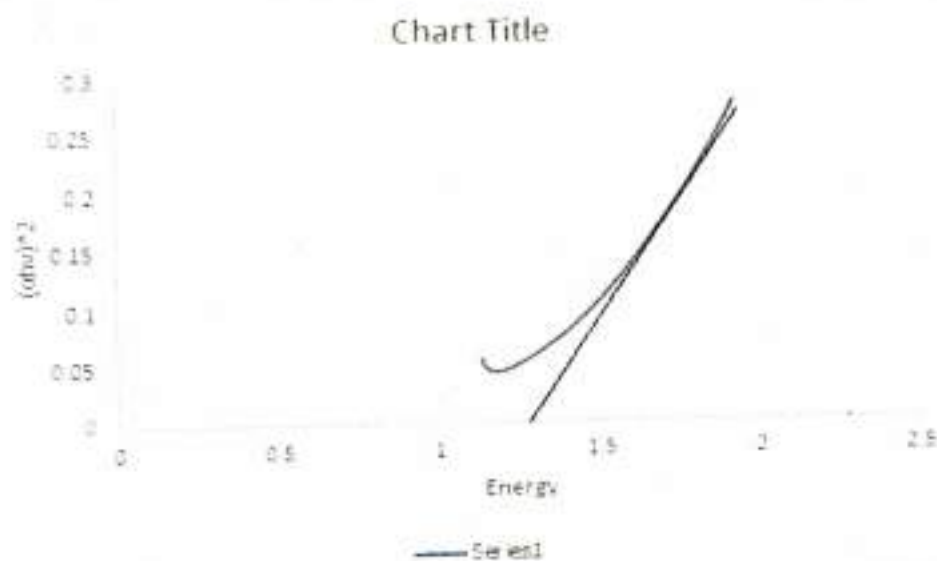


Fig. c) thickness of 30 nm (1.2 eV)

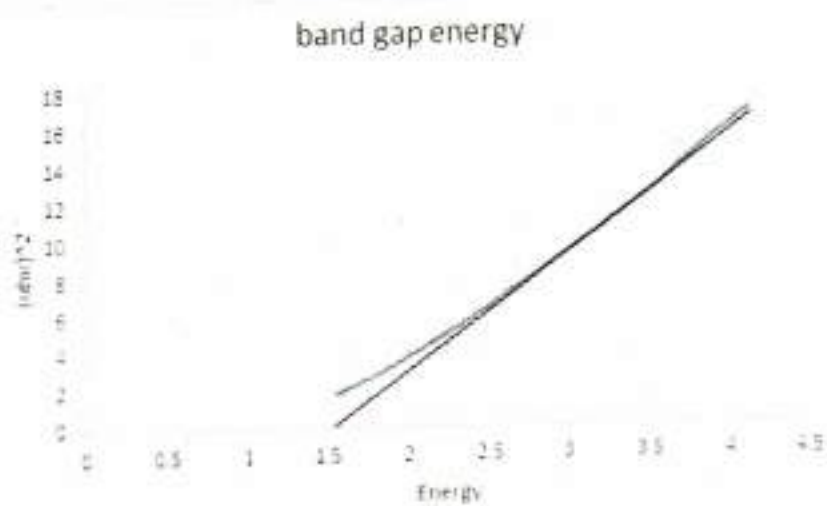
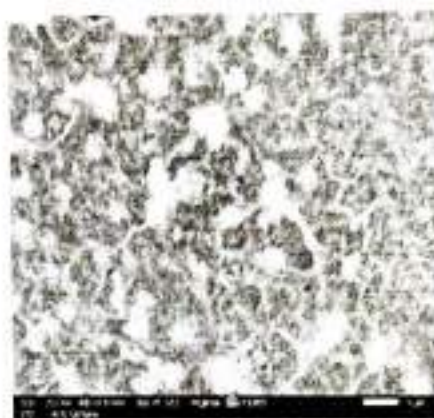
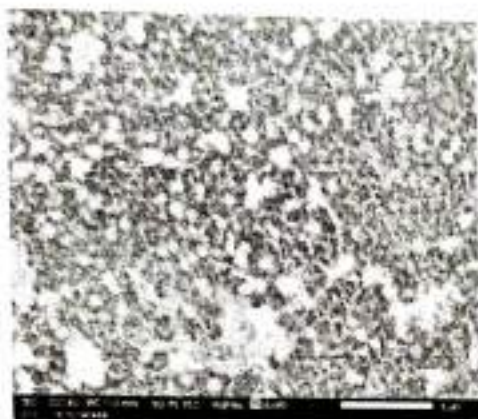


Fig. d) thickness of 1.2 nm (1.55 eV)

SEM:



Morphologies of the CuO sample were analysed by SEM and the images are displayed. The average diameter of the particle is about 1-5  $\mu\text{m}$ .

### **Conclusion-**

In this report a good quality of copper oxide thin films was successively deposited onto glass substrate using SILAR technique.

From X-Ray diffraction the crystallinity of the films increases with increase nucleation process of the precursor solution.

As the thickness of the film decreases, the band gap of material increases. This tuning of band gap can be used in several applications such as photocatalysis, solar cell, etc.

## **References:**

- ▶ Joshua O. Ighalo, Patience A. Sagboye, Great Umenweke c, Oluwaseun J. Ajala, Fredrick O. Omoarukhe,
- ▶ Comfort A. Adeyanju, Samuel Ogunniyi, Adewale G. Adeniyi, Environmental Nanotechnology, Monitoring & Management, 15, (2021).
- ▶ Gedu Sorekine, Gabriel Anduwan, Mathew Norpa Waimbo, Helen Osora, Senthilkumar Velusamy, Sungdo Kim,
- ▶ Yong Soo Kim, Junior Charles, Journal of Molecular Structure, 1248, (2021).
- ▶ S. Munyai, N.C. Hintsho-Mbita, Current research in Green and sustainable Chemistry, 4, (2021).
- ▶ Hoang Ngoc Cuong, Shreyas Pansambal, Suresh Ghotekar, Rajeshwari Oza, Nguyen Thi Thanh Hai, Nguyen
- ▶ Minh Viet , Van-Huy Nguyen, Environmental Research, 203 (2022).
- ▶ Dhananjay S Bhatkhande, Vishwas G Pangarkar and Anthony ACM Beenackers, Journal of Chemical Technology and Biotechnology, 77, (2001).
- ▶ U.G. Akpan, B.H. Hameed, Journal of Hazardous Materials 170, (2009).
- ▶ Jagpreet Singh, Vanish Kumar, Ki-Hyun Kim, Mohit Rawat, Environmental Research, 177, (2019).





**"Dissemination of Education for Knowledge, Science and Culture"**

**Shikshanmaharshi Dr. Bapuji Salunkhe**

**Fabrication of Silica-PTFE based Transparent Superhydrophobic Coating  
on Glass Substrate for Self – Cleaning and Photovoltaic Applications**

A Research Project Submitted To

**VIVEKANAND COLLEGE, KOLHAPUR (EMPOWERED AUTONOMOUS)**

FOR THE DEGREE OF MASTER OF SCIENCE

IN

PHYSICS

UNDER THE FACULTY OF SCIENCE

BY

**MISS. MAHEK SHAKILAHMED JAMADAR**

(B. Sc.)

UNDER THE GUIDANCE OF

**DR. SANJAY S. LATTHE**

(M.Sc., Ph.D.)

SELF-CLEANING RESEARCH LABORATORY,

POST GRADUATE DEPARTMENT OF PHYSICS,

**VIVEKANAND COLLEGE, KOLHAPUR (EMPOWERED AUTONOMOUS)**

(2024-2025)

### CERTIFICATE

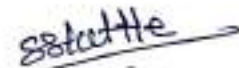
This is to certify that the project entitled "Fabrication of Silica-PTFE based Transparent Superhydrophobic Coating on Glass Substrate for Self-Cleaning and Photovoltaic Applications" being submitted herewith for the award of the degree of Master of Science in Physics under the Faculty of Science of Vivekanand College, Kolhapur (Empowered Autonomous) is the result of the original research work done by Miss. Mahek Shakilahmed Jamadar under my/our knowledge and belief the work embodied in this project has not formed earlier the basis for the award of any degree of similar title of this or any other University or Examining body.

Place: Kolhapur

Date:

  
(Dr. Sanjay S. Latthe)  
Project Guide  
Department of Physics  
Vivekanand College, Kolhapur  
(Empowered Autonomous)

  
Examiner

  
(Dr. Sanjay S. Latthe)  
Head  
Department of Physics  
Vivekanand College, Kolhapur  
(Empowered Autonomous)

### DECLARATION BY STUDENT

I hereby declare that the project entitled "**Fabrication of Silica-PTFE based Transparent Superhydrophobic Coating on Glass Substrate for Self-Cleaning and Photovoltaic Applications**" completed and written by me and has neither formed earlier the basis for the award of any degree of similar title of this nor any other University nor Examining body. Further, I declare that I have not violated any of the provisions under Copyright Privacy/Cyber/IPR Act as and when amended from time to time.

Place: Kolhapur

Date:



Miss. Mahek Shakilahmed Jamadar

Project Student

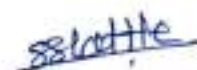


### DECLARATION BY GUIDE

This is to certify that the project entitled "**Fabrication of TEOS/MTES/PTFE based Transparent Superhydrophobic Coating on Glass Substrate for Self-Cleaning Application**" being submitted herewith for the award of the degree of Master of Science in Physics under the Faculty of Science of Vivekanand College, Kolhapur (Empowered Autonomous) is the result of the original research work done by Miss. Mahek Shakilahmed Jamadar under my/our supervision and guidance and to the best my/our knowledge and belief the work embodied in this project has not formed earlier the basis for the award of any degree of similar title of this or any other University or Examining body.

Place: Kolhapur

Date:

  
**Dr. Sanjay S. Latthe**

Project Guide

Department of Physics,  
Vivekanand College, Kolhapur  
(Empowered Autonomous)

## ACKNOWLEDGEMENT

I have great pleasure to express my deep sense of indebtedness and heart of full gratitude to my project guide Dr. Sanjay S. Latthe, Department of Physics, Vivekanand College, Kolhapur (Empowered Autonomous) for his valuable guidance given to me during the course of project work.

I am very grateful to Dr. Sanjay S. Latthe, Head of Department of Physics, Vivekanand College, Kolhapur for making available chemicals, materials, laboratory facilities and his inspiration towards a common goal of achieving scientific knowledge and pursuit it.

I wish to express my appreciation to Mr. S. S. Ingole, Mr. A. R. Jundle, Miss. R. A. Ekunde, Mr. P. P. Gaikwad for their discussion and cooperation in each and every moment of project work.

My acknowledgement will be incomplete if I don't express my appreciation towards my family members as well as my friends who helped me directly-indirectly in completion of this work successfully.



Sr. No.	Table of contents	Page No.
	<b>CHAPTER 1: INTRODUCTION</b>	
1.1	Introduction	8-9
1.2	Self-cleaning	9-10
1.3	Wettability and contact angle	10-12
	References	12-13
	<b>CHAPTER 2: METHODOLOGY AND CHARACTERIZATION TECHNIQUES</b>	
2.1	Sol-gel method	14
2.2	Modified stober method	14
2.3	Spray coating method	14
2.4	Characterizations	14-15
	References	15
	<b>CHAPTER 3: EXPERIMENTAL WORK</b>	
3.1	Materials	16
3.2	Preparation of silica sol	16
3.3	Preparation of PTFE solution	16



3.4	Spray deposition of superhydrophobic coating	16-17
	<b>CHAPTER 4: RESULT AND DISCUSSIONS</b>	
4.1	Static water contact angle and sliding angle measurements	18-19
4.2	Roughness study	19
4.3	Chemical stability	19-20
4.4	Mechanical stability	20-23
4.5	Self-cleaning ability of coated glass	24-25
4.6	Photovoltaic study of superhydrophobic coated glass cover	25-26
	<b>CHAPTER 5: CONCLUSION</b>	27

## CHAPTER 1

### INTRODUCTION

#### 1.1 Introduction

The transparent non wetting coating on glass substrates has vast applications in the field of self-cleaning surfaces. Many research groups are interested in the fabrication of self-cleaning surfaces [1]. Self-cleaning effect, also known as the lotus effect, inspired by the lotus leaf in nature. The lotus leaf has miraculous effect of self-cleaning as well as water repellent properties. Researchers observed the super power of nature and worked to mimic the effect which can be used for various applications [2]. The superhydrophobic surface is defined by its wetting character, which exhibits a static water contact angle (WCA) greater than  $150^\circ$  and a sliding angle (SA) smaller than  $10^\circ$ . Water droplets with an almost spherical shapes on superhydrophobic surfaces, carry away hydrophilic contaminants, dirt and dust particles when the droplets roll off, leaving behind the clean surface without wetting it. Superhydrophobic surfaces are governed by the chemical composition and the morphology of the surface [3]. Generally, a geometrically rough surface structure and low surface energy materials are essential for fabricating a superhydrophobic surface on a solid substrate. The superhydrophobic coating is esteemed as a promising application across diverse domains in self-cleaning, oil water separation, corrosion protection and anti-icing.

Transparent superhydrophobic coatings may be used on solar panels, building glasses, automobile, etc. Number of techniques have been documented for producing superhydrophobic surfaces including dip coating, sol gel method, spray coating and CVD. [4] Yuung et al. fabricated coating material by the TEOS/ MTES sol gel derived materials. It exhibited both superhydrophobicity resulted from the rough TEOS derived surface and hydrophobic MTES derived surface. [5] Yansheng et al. prepared superhydrophobic coating from modified  $\text{SiO}_2$  and PTFE emulsion via dip coating process.[6] Vinayak et al. studied the self-cleaning behaviour of MTMS/TEOS based silica coating by varying the amount of MTMS as a hydrophobic agent via sol gel dip coating method. Sol gel method is a novel route for the preparation of the water repellent coatings, with precise ability to control the micro structure of the deposited material to obtain surfaces with different contact angles. Prior to gelation, sol is ideal for preparing the coating. Conventionally, non-wetting, self-cleaning surfaces have been produced mainly in two ways by the sol gel method [7]. One is to create a superhydrophobic surface with a co precursor which acts as a superhydrophobic reagent and the other is to modify a surface-by-surface derivatization method. Till date, there are a few methods available on the fabrication of hydrophobic self-cleaning surface via co precursor

method that can simultaneously construct a solid surface with appropriate surface roughness and low surface energy. In recent times, modified stober method is popularly used for research purpose [8]. It is an example of a sol gel process wherein a chemical process is used to prepare silica particles of controllable and uniform size for applications in material science. In this process molecular precursor (typically TEOS) is first reacted with alcoholic solution, the resulting molecules then joining together to build larger structure [9].

In this work, we proposed a simple spray coating method to fabricate transparent superhydrophobic coating on the glass substrate using TEOS/MTES/PTFE for self-cleaning application. Initially, silica nano particles were synthesized by sol gel process using TEOS and MTES as precursors. The synthesized silica nano particles were mixed in a certain ratio with PTFE solution and stirred using a magnetic stirrer to obtain a homogenous suspension. The prepared homogenous suspension was sprayed on a glass substrate using a spray gun. The composite coating demonstrated excellent superhydrophobicity and self-cleaning performance with strong mechanical resistance. An experiment was carried out to study the photovoltaic effect with superhydrophobic glass cover on solar cell. The fill factor and efficiency of solar cell was calculated and studied.

## 1.2 Self-Cleaning Lotus Effect

The self-cleaning "lotus effect" is a fascinating phenomenon observed in the leaves of the lotus plant (*Nelumbo nucifera*). These leaves, despite growing in muddy water, remain remarkably clean. This self-cleaning property arises from the unique ultrahydrophobic (extremely water-repellent) nature of their surfaces, which is a result of a specialized micro- and nanoscopic architecture combined with a waxy coating [10].

- i. **Dual Roughness Structure:** The surface of a lotus leaf isn't smooth. It features a hierarchical structure with microscopic bumps (papillae) and even smaller nanoscopic wax crystals on top of these bumps. This creates a very rough surface at multiple scales.
- ii. **Hydrophobic Wax Coating:** The entire surface, including the micro and nano structures, is covered with a hydrophobic (water-repelling) wax.
- iii. **Minimized Contact Area:** When a water droplet lands on this rough, waxy surface, the contact area between the water and the leaf is significantly reduced. The water droplet essentially sits on the tips of the micro and nano structures, with air trapped in the valleys between them.



- iv. High Contact Angle: This minimal contact leads to a very high contact angle (typically greater than  $150^\circ$ ) between the water droplet and the leaf surface. A high contact angle signifies strong hydrophobicity.
- v. Easy Roll-Off: Due to the weak adhesion between the water droplet and the leaf surface (because of the minimal contact area), the water droplet can easily roll off the surface, even with a slight tilt or movement.
- vi. Dirt Pick-Up: As the water droplet rolls across the leaf, it adheres more strongly to loose dirt particles present on the surface than the dirt particles adhere to the leaf's micro/nanostructure. Therefore, the rolling water droplet effectively picks up and carries away dirt, dust, pollutants, and even some pathogens, leaving the leaf clean.

This remarkable self-cleaning mechanism has inspired scientists and engineers to develop various biomimetic materials and coatings with similar properties for applications such as:

- i. Self-cleaning paints and coatings: For buildings, windows, vehicles, and solar panels, reducing the need for manual cleaning.
- ii. Waterproof and stain-resistant textiles: For clothing and outdoor gear.
- iii. Anti-fouling surfaces: For medical devices and marine applications to prevent the adhesion of bacteria and other organisms.
- iv. Anti-corrosion coatings: To protect metal surfaces from moisture and environmental damage.

The lotus effect serves as a powerful example of how nature's ingenious designs can be mimicked to create innovative and practical technologies.



Figure 1.1 Self-cleaning lotus effect

### 1.3 Contact angle and wettability

The contact angle is specifically the angle between the tangent line to the liquid vapor interface and the tangent line to the solid-liquid interface at the point where all three phases meet. This angle is measured through the liquid phase.

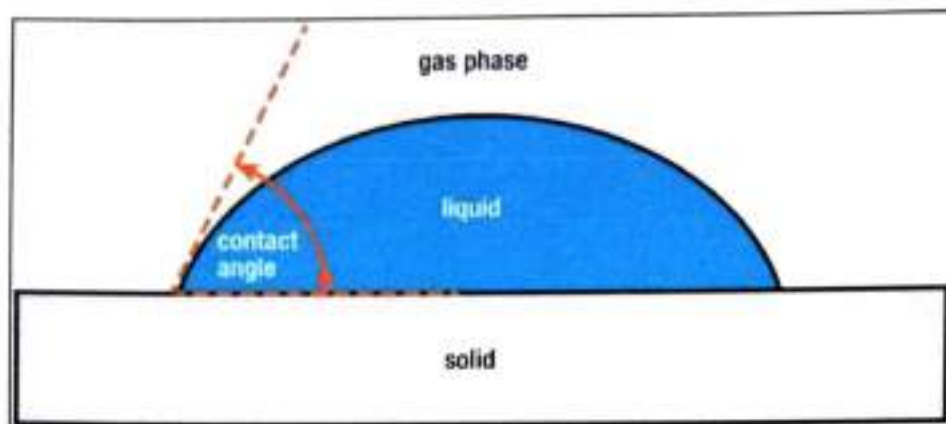


Figure 1.2. Three phase contact line of liquid on a solid surface.

Wettability is defined as the tendency of one fluid to spread on or adhere to a solid surface in the presence of other immiscible. The typical wettability is classified as hydrophilic, superhydrophilic, hydrophobic and superhydrophobic.

a) Hydrophobic surfaces

If the water contact angle is greater than  $90^\circ$  then the surface is said to be hydrophobic.

b) Superhydrophobic surfaces

If the water contact angle is greater than  $150^\circ$  then the surface becomes superhydrophobic.

c) Hydrophilic surfaces

The surface with water contact angle less than  $90^\circ$  then the surface becomes hydrophilic.

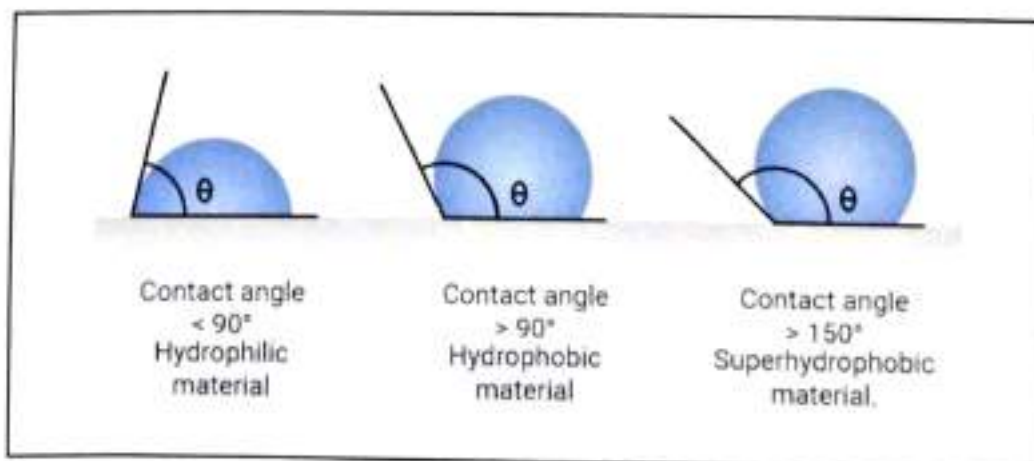


Figure 1.3. Classification of wetting based on water contact angle.

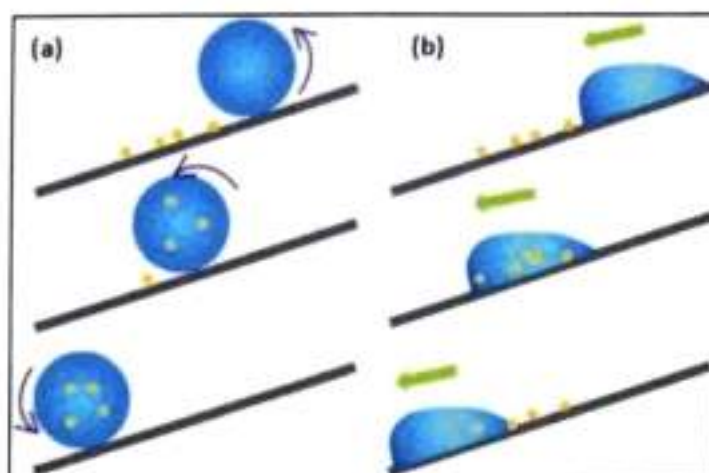


Figure 1.4. Self-cleaning process on (a) superhydrophilic surface (b) superhydrophobic surface

## References

1. "Fabrication of Superhydrophobic Coating by Spraying PDMS-SiO<sub>2</sub> Suspension for Self-cleaning Application" Sagar S. Ingole, Akshay R. Jundle, Pradip P. Gaikwad, Rutuja A. Ekunde, Rajaram S. Sutar, Sanjay S. Latthe.
2. "Superhydrophobic PVC/SiO<sub>2</sub> Coating for Self-Cleaning Application" Rajaram S. Sutar, Prashant J. Kalel, Sanjay S. Latthe, Deepak A. Kumbhar, Smita S. Mahajan, Prashant P. Chikode, Swati S. Patil, Sunita S. Kadam, V. H. Gaikwad, Appasaheb K. Bhosale, Kishor Kumar Sadasivuni, Shanhu Liu, and Ruimin Xing.
3. "Self-cleaning silica coatings on glass by single step" sol-gel route Vinayak V. Ganbavle, Uzma K.H. Bangi, Sanjay S. Latthe, Satish A. Mahadik, A. Venkateswara Rao.
4. "A convenient sol-gel approach to the preparation of nano-porous silica coatings with very low refractive indices", Yulu Zhanga, Chaoxia Zhaoa, Pingmei Wang,b Longqiang Ye,a Jianhui Luob and Bo Jianga.
5. "A Fast and Facile Fabrication of PTFE based Superhydrophobic and Ultra Wideband Angle Insensitive Anti-Reflection Coatings" Rajnarayan De, Jitendra S. Misal, Deepak D. Shinde, Shyam R. Polaki, Ranveer Singh, Tapobrata Som, Naba K. Sahoo, and K. Divakar Rao.
6. "Preparation of hydrophobic SiO<sub>2</sub>/PTFE sol and antireflective coatings for solar glass cover" Xiaoyu Sun, Lei Li, Xiaozhuang X, Guanyu Song, Jielei Tua, Pingyuan Ya, Weinan Zhang, Kai Hu.



7. "Formation of SiO<sub>2</sub>/polytetrafluoroethylene hybrid superhydrophobic coating" Yansheng Zheng, Yi He, Yongquan Qing, Zhihao Zhuo, Qian Mo.
8. "Non-fluorinated superamphiphobic surfaces through sol-gel processing of methyltriethoxysilane and tetraethoxysilane", Yuung-Ching Sheena, Wei-Hsuan Chang, Wen-Chang Chen, Yih-Her Chang, Yuan-Chang Huang, Feng-Chih Changa.
9. "Transparent superhydrophobic EVA/SiO<sub>2</sub>/PTFE/KH-570 coating with good mechanical robustness, chemical stability, self-cleaning effect and anti-icing property fabricated by facile dipping method" Meng Liu<sup>a</sup>, Xinyu Tan<sup>b</sup>, Xinyi Li<sup>a</sup>, Jialin Geng<sup>a</sup>, Mengmeng Han<sup>a</sup>, Ke Wei<sup>a</sup>, Xiaobo Chen<sup>c</sup>.
10. "Characterization and protective performance of acrylic-based nanocomposite coating reinforced with silica nanoparticles" M. Bozorg, A. Ramezani.
11. "A Convenient Sol-gel Approach to Prepare Nano-porous Silica Coatings with Very Low Refractive Indices", Yulu Zhang, <sup>a</sup>Chaoxia Zhao, <sup>a</sup>Pingmei Wang, <sup>b</sup>Longqiang Ye, <sup>a</sup>Jianhui Luo and Bo Jianga.

## CHAPTER 2

### METHODOLOGY AND CHARACTERIZATION TECHNIQUES

#### 2.1 Sol gel Method

In material science, the sol gel process is a method for producing solid materials from small molecules. The method is used for the fabrication of metal oxides, especially the oxides of silicon and titanium. The process involves conversion of monomers in solution into a colloidal solution (sol) that acts as the precursor for an integrated network (or gel) of either discrete particles or network. Typical precursors are metal alkoxides. In this method the molecular precursor is dissolved in water or alcohol and converted to gel by heating and stirring by hydrolysis /alcoholysis.

#### 2.2 Modified stober method

The modified Stöber method is a versatile technique used to synthesize monodispersed silica nanoparticles with tunable sizes and surface properties. It involves modifying the classic Stöber process by altering factors like solvent, catalyst, and reaction conditions to achieve desired particle characteristics. This method is commonly used to create silica nanoparticles with diameters ranging from 100 to 1000 nm.

#### 2.3 Spray coating method

Spray coating is a technique where a coating material is applied to a surface using a spray gun or similar device, atomizing the material into a fine mist for even distribution and a smooth, consistent finish.

Process:

**Coating Material:** The material to be sprayed can be in liquid, powder, or molten form.

**Spray Gun:** The spray gun atomizes the coating material into fine droplets, which are then directed onto the surface.

**Surface Preparation:** The surface must be adequately prepared before applying the spray coating, which may involve cleaning, sanding, or applying a primer.

**Atomization:** Compressed air or other methods are used to break down the coating material into a fine mist, allowing for even application.

#### 2.4 Characterization

The surface roughness was determined using a Stylus profiler (Mitutoyo, SJ 210, Sakado, Japan). The average roughness value was determined by recording at 3 different places. The WCA and SA were measured at 4 different places on the samples using a contact angle meter (HO-IAD-CAM-01, Holmarc Opto-Mechatronics Pvt. Ltd., Kochi, India). The average values and standard deviation of the WCA and SA of samples were noted. The mechanical durability of the coatings was evaluated by adhesive tape test, sand paper abrasion test, water droplet test, sand particle impact test and pencil hardness test. The chemical stability of the coating was evaluated by the acid-base immersion test. The self-cleaning property of the coating was determined using chalk powder, soil particles and muddy water as a contamination. The fill factor and efficiency of solar cell using coated glass was calculated by performing the photovoltaic study experiment.

## References

1. "Fabrication of Superhydrophobic Coating by Spraying PDMS-SiO<sub>2</sub> Suspension for Self-cleaning Application" Sagar S. Ingole, Akshay R. Jundale, Pradip P. Gaikwad, Rutuja A. Ekunde, Rajaram S. Sutar, Sanjay S. Latthe.
2. "Superhydrophobic PVC/SiO<sub>2</sub> Coating for Self-Cleaning Application" Rajaram S. Sutar, Prashant J. Kalel, Sanjay S. Latthe, Deepak A. Kumbhar, Smita S. Mahajan, Prashant P. Chikode, Swati S. Patil, Sunita S. Kadam, V. H. Gaikwad, Appasaheb K. Bhosale, Kishor Kumar Sadasivuni, Shanhu Liu, and Ruimin Xing.
3. "Self-cleaning silica coatings on glass by single step" sol-gel route Vinayak V. Ganbavle, Uzma K.H. Bangi, Sanjay S. Latthe, Satish A. Mahadik, A. Venkateswara Rao.
4. "A convenient sol-gel approach to the preparation of nano-porous silica coatings with very low refractive indices", Yulu Zhanga, Chaoxia Zhaoa, Pingmei Wang,b Longqiang Ye,Jianhui Luo and Bo Jianga.
5. "A Fast and Facile Fabrication of PTFE based Superhydrophobic and Ultra Wideband Angle Insensitive Anti-Reflection Coatings" Rajnarayan De, Jitendra S. Misal, Deepak D. Shinde, Shyam R. Polaki, Ranveer Singh, Tapobrata Som, Naba K. Sahoo, and K. Divakar Rao.
6. "Preparation of hydrophobic SiO<sub>2</sub>/PTFE sol and antireflective coatings for solar glass cover" Xiaoyu Sun, Lei Li, Xiaozhuang X, Guanyu Song, Jielei Tua, Pingyuan Ya, Weinan Zhang, Kai Hu.



## CHAPTER 3

### EXPERIMENTAL DETAILS

#### 3.1 Materials

Tetraethyl orthosilicate (TEOS 98%), Methyltriethoxysilane (MTES 99%), Polytetrafluoroethylene (PTFE) were obtained from Sigma Aldrich (Bangalore, India).  $\text{NH}_4\text{OH}$  solution 25% was bought from Research Lab Fine Chem Industries (Mumbai, India). Ethanol (99.9%) was purchased from Laboratory Solutions, India. The microscope slides (25.4 mm  $\times$  76.2 mm, 1 mm – 1.2 mm thick) were obtained from Riviera, India. Double distilled water was prepared in the laboratory and used as it is.

#### 3.2 Preparation of silica sol

Initial silica sol was synthesized by the modified Stöber method. 10 mL of ethanol was used as solvent in a round bottom flask. (It was placed in a beaker containing water of which the water level was adjusted to the level below the level of the solvent). The solvent was heated at the temperature 55°C along with magnetic stirring at 250 rpm. After the temperature of the solvent attained desired temperature, 0.6 mL of the TEOS and 0.6 mL of  $\text{NH}_4\text{OH}$  was added dropwise. The solution was continuously stirred and heated. After 1 h of stirring, 0.6 mL of MTES was added to the mixture. After 2 h of adding MTES, heating was switched off and stirring was continued for 2 days. Thus, the silica sol was obtained, labelled as solution A.

#### 3.3 Preparation of (PTFE) sol

50  $\mu\text{L}$  of PTFE was added to 5 mL of double distilled water. The solution was stirred for 1 h. This PTFE solution obtained was labelled as solution B.

#### 3.4 Spray deposition of Superhydrophobic solution

The glass slides were used as substrates and pretreatment was given to the glass slide before coating, in order to remove contaminants, present on the surface. The glass slides were soaked in labolene solution for 1 h and then thoroughly rinsed under tap water. These slides were then cleaned in ultrasonic bath for 20 min, followed by rinsing with deionized water in turn to remove the surface contamination and dust. At last, all the glass slides were dried at 80°C for 30 min in the hot air oven and were then used for fabrication process.

The solution for spray deposition was prepared by mixing the solution A and solution B. In 1.5 mL of solution A, solution B was added. The concentration of solution B was varied

as 0, 0.25, 0.5 and 0.75 mL. The mixture was stirred for 10 min at 100 rpm. Thus, the white viscous liquid was obtained. The mixture was directly coated on glass substrate via spray coating process, the clean substrate was clamped to the holder and the solution was sprayed by a spray gun. The approximate distance between tip of the nozzle of spray gun and substrate was kept fixed at 10 cm, pressure 2 bar and nozzle diameter 0.3mm. Thus, the transparent coating was obtained. The spray coated samples were labelled as MT, MP1, MP2 and MP3 respectively. Then the coating was heated at 100°C for 1 h to remove residual solvent. Finally, uniform coating was formed after heating.

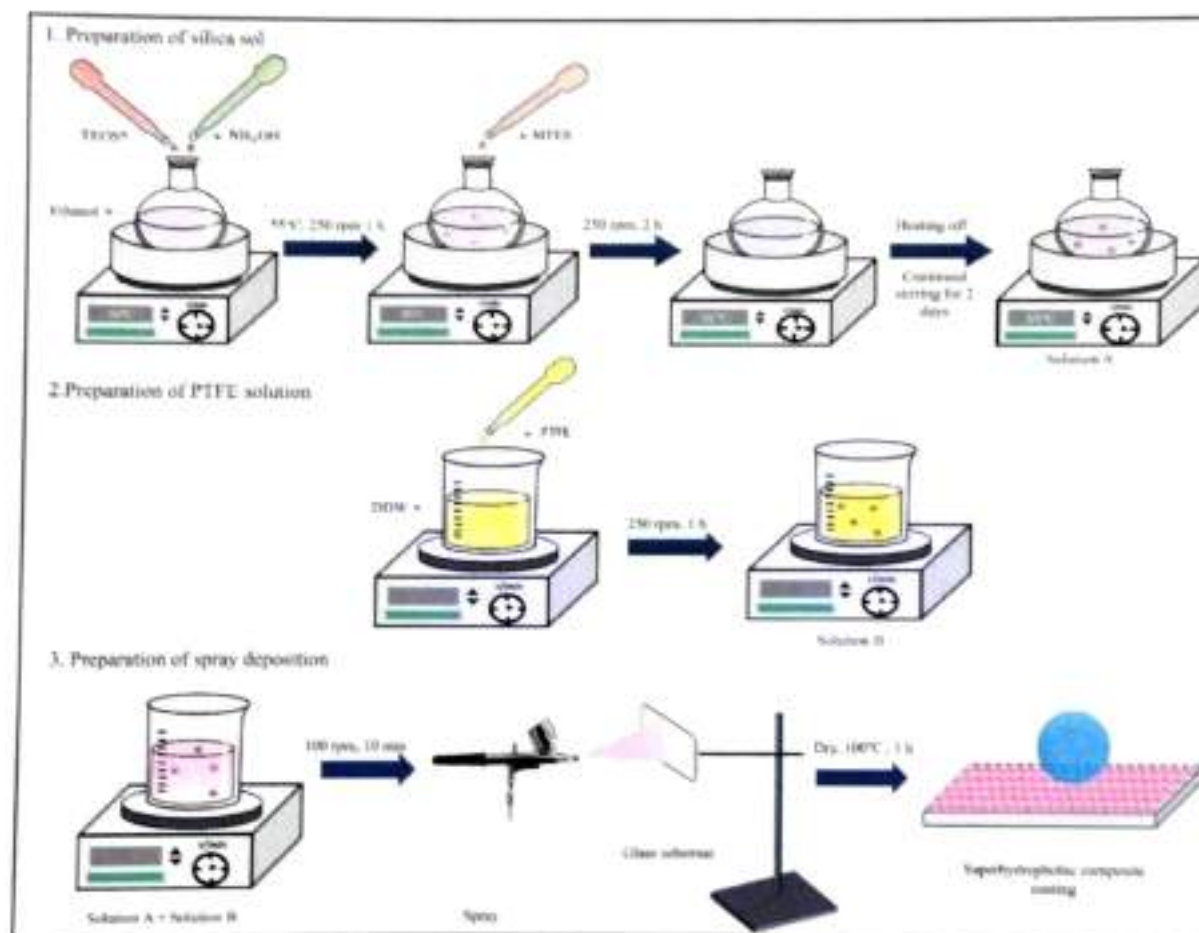


Figure 3.1. Schematic of preparation of superhydrophobic coating on glass substrate

## CHAPTER 4

## RESULTS AND DISCUSSION

## 4.1 Static water contact angle and sliding angle measurements

The static contact angles and sliding angles are measured to study the wetting and self-cleaning property of the hydrophobic silica coatings. The clean glass slide show the water contact angle of  $35^\circ$ , indicating hydrophilic surface. For coated glass MT sample show the WCA and SA of  $161^\circ$  and  $2^\circ$  respectively revealing the superhydrophobic nature. The WCA measured for MP1 sample was  $155.8^\circ$  and sliding angle was  $3^\circ$ . The MP2 sample exhibited a WCA of  $162^\circ$  and SA of  $3^\circ$ , figure (4.1) though slightly less effective than MP1. Similarly, the MP3 sample displayed a WCA of  $148.3^\circ$ , figure (4.4). Figure (4.2) provides an optical image of colored water droplets on the MP2 samples, demonstrating the superhydrophobic effect visually. Additionally, figure (4.3) shows the transparency of the coated samples.



Figure 4.1. Water contact angle image of MP2 sample      Figure 4.2. Optical image of colored water droplets on MP2 sample



Figure 4.3. Optical image of (a) uncoated sample (b) MT sample (c) MP1 sample (d) MP2 sample (e) MP3 sample



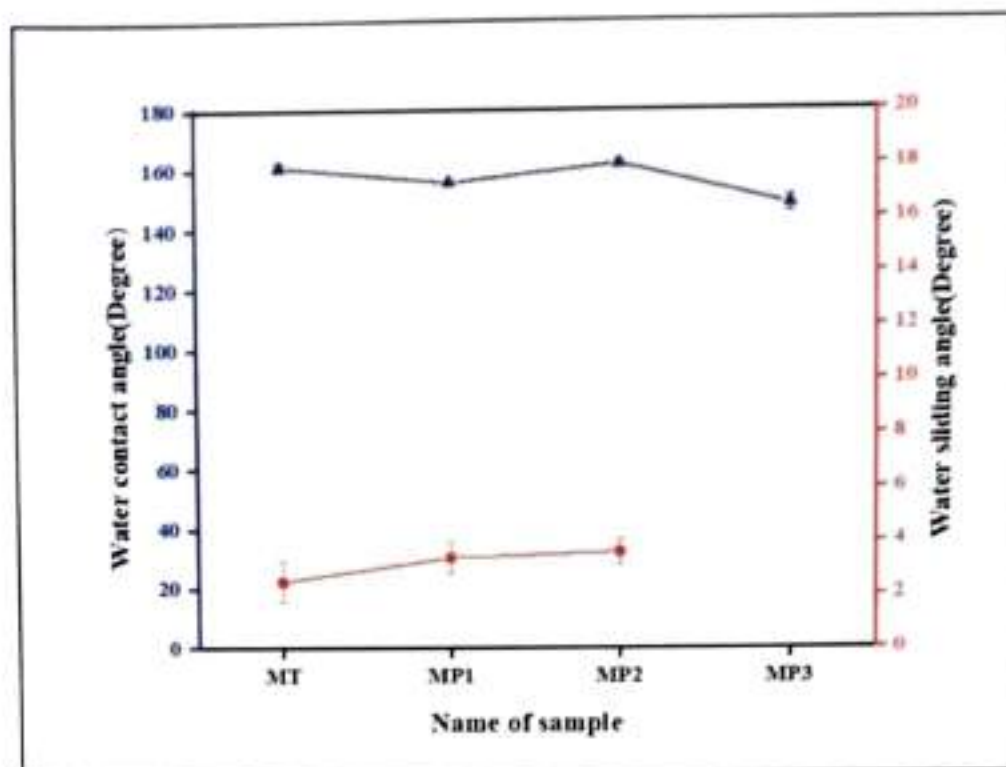


Figure 4.4. Graph of WCA and WSA of the samples

#### 4.2 Roughness study

The wettability of the surface is decided by the roughness of the coatings. The surface values of clean glass slide and coated samples were measured. As far as the morphology of a surface is concerned, hydrophobicity of hydrophobic surface is well known to be enhanced with increase in roughness. We measured the surface roughness and observed that roughness value of clean glass slide is  $0.02 \mu\text{m}$ , for MT1 it is  $0.203 \mu\text{m}$ . Similarly for the samples MP1, MP2, and MP3, roughness values recorded were  $0.120 \mu\text{m}$ ,  $0.211 \mu\text{m}$ ,  $0.101 \mu\text{m}$ . We can see that there is a decrease in the contact angle as surface roughness decreased which agree well with the theoretical aspects.

#### 4.3 Chemical Stability

The chemical stability of superhydrophobic coating is very important for their practical applications. Here the chemical stability of the TEOS/MTES/PTFE coating was evaluated by the wetting property of the coating after immersion in strong acid/alkali solution. The HCl solution (pH3) and  $\text{NH}_4\text{OH}$  solution (pH11) was prepared in a beaker. Small pieces of the substrates were immersed in two beakers. The substrates were kept immersed for 20 min, took out of the solutions and dried for 10 minutes at  $60^\circ \text{C}$  in the hot air oven, then measure water contact angle of each substrate. This process was repeated until immersion time of 100 minute

and WCA has been recorded each time, figure (4.5). It can be seen that there is no much loss of super hydrophobicity of the coatings in acid/alkali solution indicating that it can well expose to the chemicals.

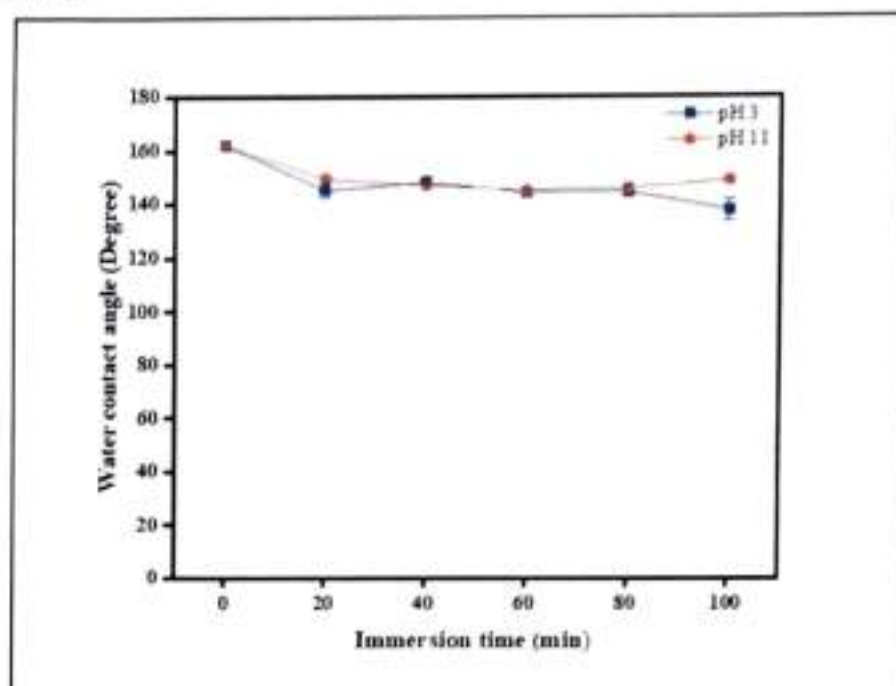


Figure 4.5. Graph of acid-base immersion test.

#### 4.4 Mechanical stability

To evaluate the practical applicability in outdoor exposure, it is essential to determine the mechanical stability of the prepared samples. For this purpose, adhesive tape peeling test, sand paper abrasion test, water droplet impact test, sand particles impact test and pencil hardness test were carried out. The adhesiveness of the prepared coating toward the substrate was evaluated by the adhesive tape test. An adhesive tape was applied to the MP2 sample and a metallic disc weighing 50 g was rolled on it for 1 min to remove the air gap between the substrate and tape. Afterward, the tape was torn off from the substrate, which was considered a cycle. The WCAs were measured after each cycle. It was observed that the WCA decreased to  $91^\circ$  after 4 cycles, indicating some detachment of the coating material which adhered to the tape. The variation of WCA after each cycle is depicted in figure (4.6), and the optical photograph of the experimental setup for the adhesive tape peeling test is shown in the inset figure (4.6).

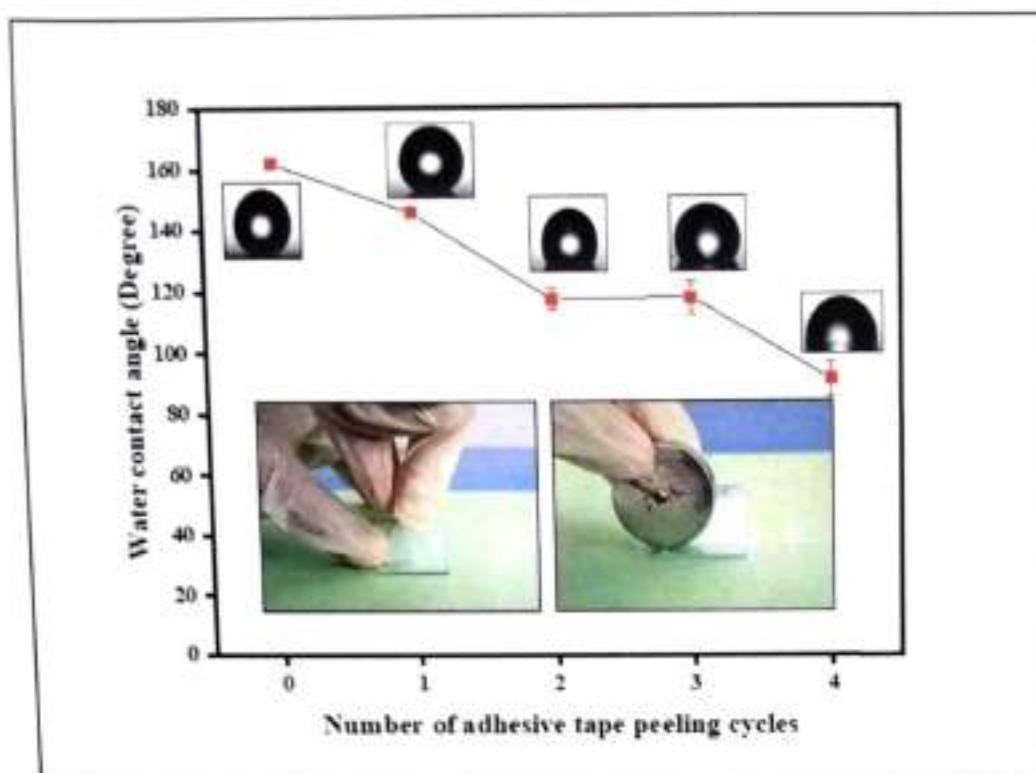


Figure 4.6. Graph of adhesive tape peeling test on MP2 sample.

In large scale applications superhydrophobic coatings can be damaged by scratch, rubbing and finger contact. To sustain the hierarchical micro/ nano structure and low surface energy of superhydrophobic coating under mechanical abrasion is one of the important issues. The mechanical abrasion test was performed using sandpaper grit number 100CW. The coated surface of the PS2 sample was placed on sandpaper with a 20 g weight loaded on top. For one cycle of sandpaper abrasion, the sample was dragged for 15 cm at a normal speed. After each cycle, the WCA was recorded to evaluate the mechanical stability of the coating. Fortunately, the WCA was recorded as  $143^\circ$  after 6 cycles. Post-test, the coated surface from the sample appeared partially removed and observed on the sandpaper surface. The reduction in WCA after each cycle is depicted in figure (4.7), along with an optical image of the experimental setup in the inset.



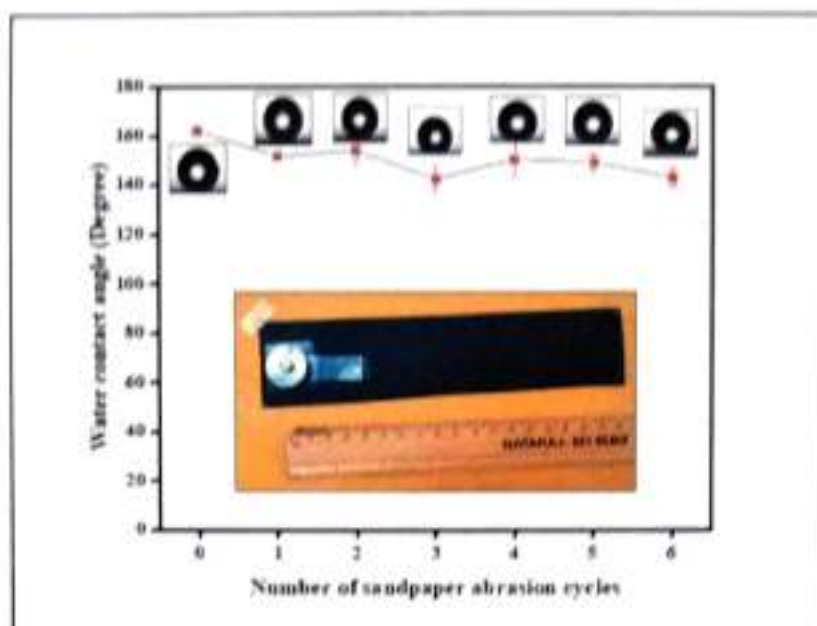


Figure 4.7. Graph of sandpaper abrasion test on MP2 sample.

Furthermore, water droplet impact test was carried out, photographic set up of which can be seen in figure (4.8a). The superhydrophobic coating with an inclination angle of  $45^\circ$  is placed at a height of 25 cm below the faucet and the water droplets are released continuously at a controllable rate. The WCA was recorded for every 50 ml of water. Due to continuous impact of water drops, coating loses its superhydrophobicity which results in decrease of WCA, figure (4.8b). The WCA was reduced to  $93^\circ$  for impact of 400 ml of water.

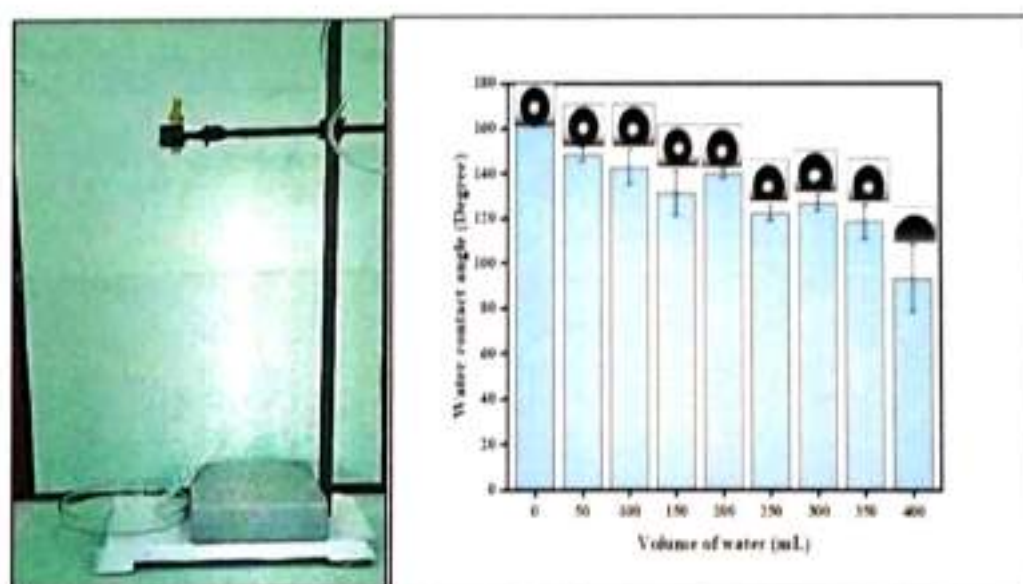


Figure 4.8. (a) Optical image of experimental set up of water droplet test on MP2 sample. (b) Graph of water droplet test.

The sand particle impact test is visually shown in figure (4.9a). The coated piece of sample was placed in a petri dish with an inclination angle of  $45^\circ$  was impacted with 2 g of grit (the distance between the grits and the coating is about 40 cm). The WCA was noted after every impact. It was observed, WCA slowly went on decreasing after each cycle and reached  $130^\circ$  for 12 g of sand, figure(4.9b). From this we can know that the coating is of good strength confirming good mechanical stability.

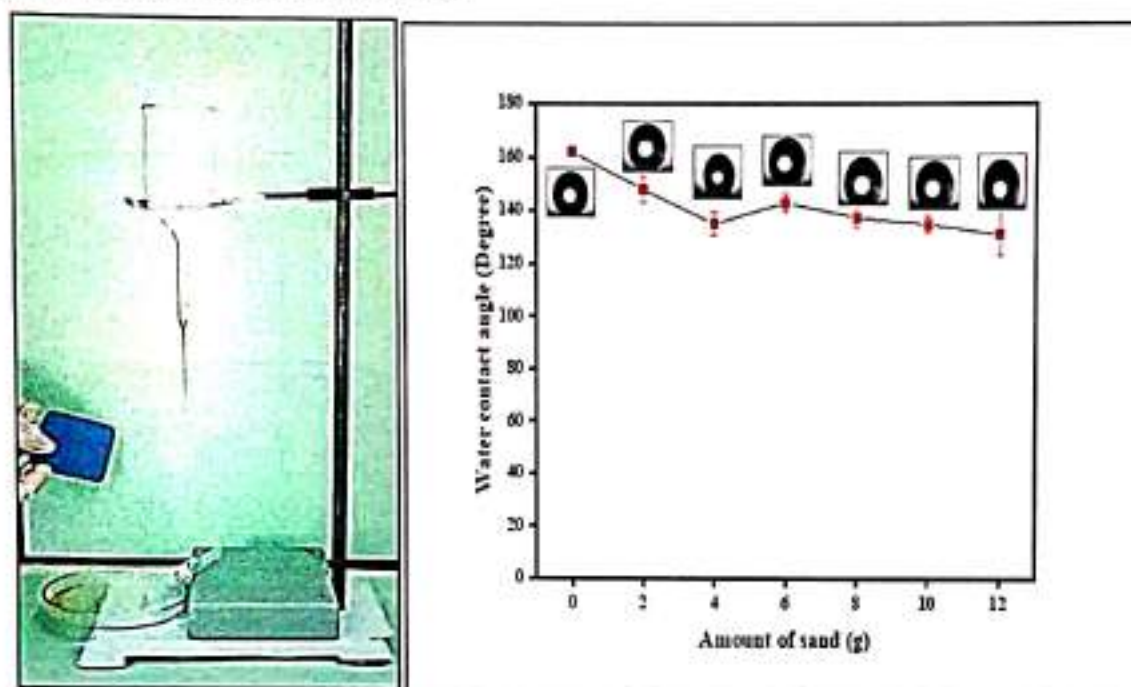


Figure 4.9. (a) Optical image of experimental set up of sand particles impact test on MP2 sample. (b) Graph of sand particles impact test.

To evaluate the scratch resistance and hardness of coatings, pencil hardness test was performed. During the test, a 6B pencil tip was used with a pressure of 500g applied to the surface. The tester was dragged across the coating, and it was observed that the dragged area underwent complete removal, leaving no discernible coated layer. (As shown in figure 4.10).

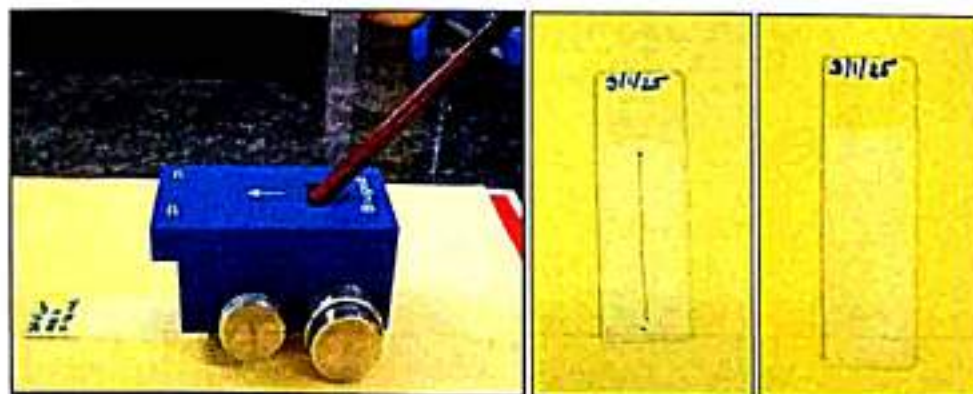


Figure 4.10. Pencil hardness test conducted on MP2 sample.



#### 4.5 Self-cleaning

An intrinsic property of the self-cleaning superhydrophobic surface is its ability to repel water droplets, causing them to roll off the surface and carry away contaminants, just like a lotus leaf. To assess the self-cleaning performance of the MP2 sample, it was kept in petri dish and chalk powder was uniformly sprinkled over the surface. Following this, water droplets were gently applied to the dust-contaminated surface using a dropper. The water droplets, upon contact with the surface immediately picked up the chalk particles due to the low adhesion between the surface and the contaminants. This interaction caused the water droplets to bead up and roll off the surface, effectively removing the chalk powder and leaving behind a clean and uncontaminated surface. The process was repeated multiple times to ensure consistency and reliability of the self-cleaning performance. As illustrated in figure (4.12), the sequence of images captures the progression of the water droplets as they collect and remove the chalk powder from the surface. Similar process was carried out by the fine soil particles over the coating as seen in the figure (4.11).

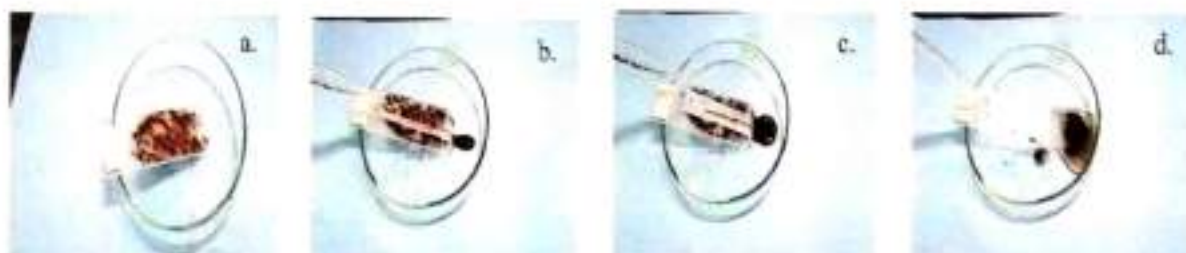


Figure 4.11. (a-d) Self-cleaning performance of the MP2 sample against soil dust

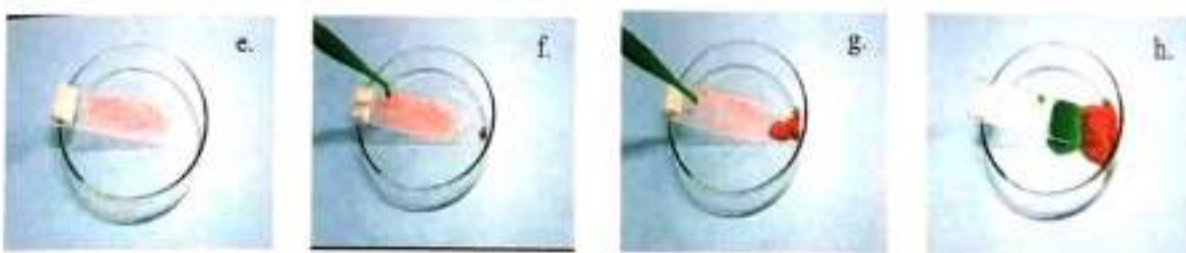


Figure 4.12. (e-h) Self-cleaning performance of the MP2 sample against chalk powder

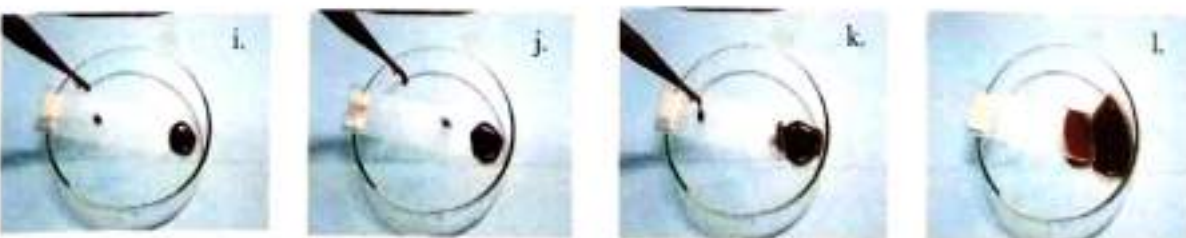


Figure 4.13. (i-l) Self-cleaning performance of the MP2 sample against muddy water



Further, the self-cleaning ability of the prepared superhydrophobic coating was also tested by muddy water. The muddy water was prepared by dispersing fine soil particles in water. Fine particles of soil of about 15 g were dispersed in 25 ml of water in a beaker. This muddy water was dropwise poured on the coating by using a dropper. In the process of pouring muddy water, it eventually gets repelled off the superhydrophobic coating, figure (4.13). The coating exhibited exceptional self-cleaning properties, demonstrating its capability to maintain cleanliness with minimal effort. The performance can be attributed to the high-water contact angle and low sliding angle of the coating which facilitate the easy rolling off of water droplets thereby ensuring efficient removal of contaminants. The robust self-cleaning ability of the MP2 sample highlights its potential for application in environment where maintaining surface cleanliness is critical, such as in outdoor structures, automotive surfaces and electronic devices.

#### **4.6 Photovoltaic study by using superhydrophobic coated glass cover**

Superhydrophobic coatings on photovoltaic glass cover enhance self-cleaning and reduce dust accumulation, improving photovoltaic module efficiency by preventing dust and debris accumulation and improving water droplet removal. These coatings often transparent, repel water and dirt, promoting easy cleaning and maximizing sunlight absorption, leading to power generation. It is best to install in arid and dry areas. An experiment was conducted to study the fill factor and efficiency of solar cell by using TEOS/ MTES/PTFE coated glass cover. The optical photograph of the experimental setup is shown in the figure. The ammeter, voltmeter, load resistance and solar cell were connected in circuit. The distance between bulb of the lamp and solar cell was kept fixed at 30 cm. The solar cell was inclined at an angle of  $30^\circ$ . Firstly, the light was incident on the bare solar cell, then ammeter and voltmeter readings were noted. The fill factor and efficiency of solar cell were calculated which is 0.6359 and 4.870% respectively. Next, the superhydrophobic coated glass (size) was fixed on the solar cell and then light was incident on it. The value of fill factor and efficiency measured for this is 0.4946 and 3.2470% respectively. For further studies, we had sprinkled soil particles as debris on the coated surface and the procedure was repeated. The fill factor for this condition is found to be 0.5806 and the efficiency is 3.17%. At last, after self-cleaning of surface was performed, we calculated fill factor is 0.55 and efficiency is 3.92%. The experiment confirm that TEOS/MTES/PTFE coated transparent superhydrophobic glass on solar cell should be promoted as it is easy cleaning which reduces the cost of maintenance and also increases the power generation by maximum absorption of sunlight by the photovoltaic cell.



Figure 4.14. Photovoltaic study by using superhydrophobic glass cover



## CHAPTER 5

### CONCLUSION

In conclusion, we have successfully fabricated a transparent self-cleaning superhydrophobic coating on a glass substrate using a facile sol gel spray coating method. The self-cleaning behaviour of TEOS/MTES based silica coating varying the amount of PTFE hydrophobic agent was studied. The synthesized MP2 coating exhibited a high-water contact angle of  $162^\circ$  indicating excellent water repellency and low sliding angle of  $3^\circ$  confirming its superior self-cleaning ability. Moreover, the chemical stability of the coating was estimated by acid base immersion test. The mechanical stability of the coating was rigorously tested through multiple adhesive tape peeling test, sandpaper abrasion test, water drop impact and sand particle impact test as well as pencil hardness test. The results demonstrated that the coating maintained its superhydrophobic properties and structural integrity under these conditions indicating strong chemical and mechanical resistance. Additionally, the self-cleaning performance was evaluated using chalk powder, soil particles and muddy water, the coating effectively repelled contaminants without losing its superhydrophobic properties. Furthermore, experiments under the actual working condition of photovoltaic cell also show that the coating is indeed self-cleaning which can improve the efficiency of the photovoltaic panels and lower the temperature of the photovoltaic panels, thus reducing the expenditure on cleaning and maintenance and improving the service life of the photovoltaic panels. This technique provides a new opportunity in the practical application of self-cleaning film on photovoltaic glass covers. The study highlights the potential of the superhydrophobic coating for practical applications particularly in the environment, where maintaining cleanliness and minimizing contamination are crucial. The scalability and simplicity of the spray coating method further enhance its applicability for large production. This research opens new avenues for developing advanced self-cleaning surfaces, which can significantly benefit industries such as construction, automotive and consumer electronics by reducing maintenance cost and improving product longevity.